

# Dynamical Zodiacal Cloud Models Constrained by High Resolution Spectroscopy of the Zodiacal Light

Sergei I. Ipatov <sup>a,b,\*</sup>, Alexander S. Kutyrev <sup>c</sup>, Greg J. Madsen <sup>d,1</sup>, John C. Mather <sup>c</sup>,  
S. Harvey Moseley <sup>c</sup>, Ronald J. Reynolds <sup>e</sup>

<sup>a</sup> *Department of Terrestrial Magnetism of Carnegie Institution of Washington, 5241 Broad  
Branch Road, Washington, DC, 20015-1305, USA*

<sup>b</sup> *Space Research Institute, 84/32 Profsoyuznaya st., Moscow, 117997, Russia*

<sup>\*</sup> *Corresponding Author E-mail address: siipatov@hotmail.com*

<sup>c</sup> *NASA/GSFC, Greenbelt, MD 20771*

<sup>d</sup> *Anglo-Australian Observatory, P.O. Box 296, Epping, NSW 1710, Australia*

<sup>e</sup> *Department of Astronomy, 475 North Charter st., University of Wisconsin at Madison,  
Madison, WI 53706, USA*

Pages: 45

Tables: 2

Figures: 8

arXiv:0711.3494v1 [astro-ph] 22 Nov 2007

---

<sup>1</sup>NSF Distinguished International Postdoctoral Research Fellow

**Proposed Running Head:** Dynamical zodiacal cloud models

Ipatov et al.

**Editorial correspondence to:**

E-mail address: siipatov@hotmail.com

Dr. Sergei Ipatov, 22 Parkway rd., Apt. A, Greenbelt, MD 20770

## ABSTRACT

The simulated Doppler shifts of the solar Mg I Fraunhofer line produced by scattering on the solar light by asteroidal, cometary, and trans-Neptunian dust particles are compared with the shifts obtained by Wisconsin H-Alpha Mapper (WHAM) spectrometer. The simulated spectra are based on the results of integrations of the orbital evolution of particles under the gravitational influence of planets, the Poynting-Robertson drag, radiation pressure, and solar wind drag. Our results demonstrate that the differences in the line centroid position in the solar elongation and in the line width averaged over the elongations for different sizes of particles are usually less than those for different sources of dust. The deviation of the derived spectral parameters for various sources of dust used in the model reached maximum at the elongation (measured eastward from the Sun) between  $90^\circ$  and  $120^\circ$ . For the future zodiacal light Doppler shifts measurements, it is important to pay a particular attention to observing at this elongation range. At the elongations of the fields observed by WHAM, the model-predicted Doppler shifts were close to each other for several scattering functions considered. Therefore the main conclusions of our paper don't depend on a scattering function and mass distribution of particles if they are reasonable. A comparison of the dependencies of the Doppler shifts on solar elongation and the mean width of the Mg I line modeled for different sources of dust with those obtained from the WHAM observations shows that the fraction of cometary particles in zodiacal dust is significant and can be dominant. Cometary particles originating inside Jupiter's orbit and particles originating beyond Jupiter's orbit (including trans-Neptunian dust particles) can contribute to zodiacal dust about 1/3 each, with a possible deviation from 1/3 up to 0.1-0.2. The fraction of asteroidal dust is estimated to be  $\sim 0.3-0.5$ . The mean eccentricities of zodiacal particles located at 1-2 AU from the Sun that better fit the WHAM observations are between 0.2 and 0.5, with a more probable value of about 0.3.

**Key Words:** Asteroids; Comets, dust; Trans-Neptunian objects; Spectroscopy; Zodiacal light

## 1. Introduction

A lot of dust particles are produced by small bodies in the solar system. The dust located within about 2 AU from the Earth is seen as the zodiacal light. There are various points of view on the contributions of asteroidal, cometary, and trans-Neptunian dust to the zodiacal cloud. The estimates of the contributions made in several works are summarized in Table 1. These estimates were based on the Infrared Astronomical Satellite (*IRAS*) and *COBE/DIRBE* observations, on cratering rates, shape of microcraters, etc. In the present paper, for estimates of the contributions we analyzed some of these observations using our studies of migration of dust particles produced by different small bodies. We considered a wide range of particle masses, whereas some other scientists used results of calculations for one or two sizes of particles, e.g., Liou et al. (1995) considered 9  $\mu\text{m}$  diameter dust particles, and studies by Gorkavyi et al. (2000a,b) and Ozeroy (2001) were based on 1  $\mu\text{m}$  and 5  $\mu\text{m}$  particles modeling. In our analysis for the first time we use the observations of velocities of zodiacal dust particles obtained by Reynolds et al. (2004) with the use of the Wisconsin H-Alpha Mapper (WHAM) spectrometer.

To set the stage for our work we first review some published estimates of asteroid/cometary contributions to the zodiacal cloud in more detail than in Table 1. A significant fraction of cometary dust in the near-Earth space was proposed by Southworth (1964), Liou et al. (1995), and Zook (2001). Based on cratering rates from an ensemble of Earth- and Lunar-orbiting satellites, Zook (2001) estimated that the cometary contribution to the near-Earth flux of particles is  $\sim 75\%$ . His conclusion was based on (1) the comparison of the meteoroid penetration rates of the 25- $\mu\text{m}$  thick cells of the Earth-orbiting *Explorer 16* and *23* satellites with the penetration rate of the five *Lunar Orbiter* satellites that had nearly identical cells of the same thickness and on (2) the studies of the crater production rate on the leading edge of the Earth-orbiting Long Duration Exposure Facility (*LDEF*) satellite, as compared to that on the trailing edge. For the estimates of the cometary contribution, Zook also used (1) Humes’s (1993) result that it takes a mean Earth-entry velocity of about 17  $\text{km s}^{-1}$  to give agreement with the *LDEF* observations and (2) Jackson and Zook’s (1992) numerical modeling, which showed that meteoroids originating in the main belt of asteroids will strike the top of the Earth’s atmosphere with a mean velocity between 12 and 13  $\text{km s}^{-1}$ .

< Place for Table 1 >

Grogan et al. (2001), Dermott et al. (2001), and Wyatt (2005) suggested that at least 30% of zodiacal dust comes from the break-up of asteroids in order to explain formation of dust bands (i.e., excesses of dust at elliptic latitudes  $\leq 10^\circ$  (Kelsall et al. 1998)), as dust bands alone supply as much as 30%. Kortenkamp and Dermott (1998) suggested that the Earth predominately accretes asteroidal dust. Dermott et al. (2002) concluded that most of

zodiacal dust particles can be of asteroidal origin and have eccentricities  $e < 0.1$ . Grün (1994) and Grün et al. (2001) considered that zodiacal particles orbit the Sun at low inclination ( $i < 30^\circ$ ) and moderate eccentricity ( $e < 0.6$ ) orbits. Our studies presented in Section 4 are in accordance with Grün’s estimates.

Nesvorný et al. (2006) compared the *IRAS* observations with their computer model of the thermal emission of the Karin and Veritas family particles. Their best-fit model results suggest that the Karin and Veritas family particles contribute by 5-9% in 10-60- $\mu\text{m}$  wavelengths to the zodiacal brightness within  $50^\circ$  latitudes around the ecliptic, and by 9-15% within  $10^\circ$  latitudes. The high brightness of the zodiacal cloud at large latitudes suggests that it is mainly produced by particles with higher orbital inclinations than what would be expected for asteroidal particles produced by sources in the main asteroid belt. Based on these results, Nesvorný et al. infer that asteroidal dust represents a smaller fraction of the zodiacal cloud than previously thought (e.g., by Dermott et al., 2001). They hypothesize that up to  $\approx 50\%$  of interplanetary dust particles measured by the *LDEF* may be made up of particles species from the Veritas and Karin families. Based on their modelling, the disproportional contribution of Karin/Veritas particles to the zodiacal cloud (only 5-9%) and to the terrestrial accretion rate (30-50%) suggests that the effects of gravitational focusing by the Earth enhance the accretion rate of Karin/Veritas particles relative to those in the background zodiacal cloud. Nesvorný et al. (2006) noted that the size distribution of asteroidal particles can be a strong function of the heliocentric distance. They infer that the zodiacal cloud emission may be dominated by high-speed cometary particles, while the terrestrial impactor flux contains a major contribution from asteroidal sources. Hahn et al. (2002) concluded that, though about 80% of the dust particles in the sample of dust collected in the Earth’s stratosphere by U2 aircraft (Brownlee et al. 1993) have low entry velocities consistent with asteroidal orbits, the dust released from low-inclination Jupiter-family comets can also have low entry velocities, and the Earth’s gravitational focusing naturally selects for low-velocity dust over all dust.

Sykes et al. (2004) infer that the zodiacal cloud scale height is not a good discriminator between asteroids and comets as the main supply of dust because inclinations of some Jupiter-family comets are not very different from those for asteroids and the half-width of the distribution of asteroidal orbital inclinations ( $12^\circ$ - $16^\circ$ ) does not differ much from the half-width ( $14^\circ$ ) at half-maximum number density for the Kelsall model. Some models based on *in situ* particle detections suggest that the inclination distribution may have a half-width as wide as  $20^\circ$ - $30^\circ$  (Dikarev et al. 2002). If the latter estimate is true, then the fraction of zodiacal dust produced by long-period comets can exceed 10-20%.

Landgraf et al. (2002) concluded that Comet 29P/Schwassmann-Wachmann 1 itself is

able to provide a major fraction of the solar system dust that is currently found between 6 and 8 AU. Comparison of the number density of dust particles produced by different small bodies with the observed constant density of  $\sim 10 \mu\text{m}$  particles between 3 and 18 AU (Humes 1980, Grün 1994) showed (Ozernoy 2001; Landgraf 2002; Ipatov and Mather 2006) that a considerable fraction of dust at such distances is produced by comets. The conclusions on a considerable fraction of cometary dust are also in agreement with earlier studies of the dynamics of Jupiter-family comets (Ipatov and Mather 2003, 2004a-b, 2006), which showed that some former cometary objects could get high eccentric orbits located entirely inside Jupiter’s orbit and stay in these orbits for a long time. Some of these objects could disintegrate producing a substantial amount of dust.

Grün et al. (1985) proposed that the main contribution to the zodiacal light is from particles that range from 20 to 200  $\mu\text{m}$  in diameter (for silicate particles, this range corresponds to the ratio of the Sun’s radiation pressure force to gravitational force  $\beta \sim 0.002\text{-}0.02$ ). The cratering record on *LDEF* showed (Love and Brownlee 1993) that the cross-sectional area distribution of particles accreted by the Earth reaches maximum at a particle diameter  $d \sim 100 \mu\text{m}$ . Smaller particles have a larger surface per unit of mass of particles. For a fragmentation power law  $n(r_p)dr_p = n_0 r_p^{-q} dr_p$ , the brightness of produced particles is proportional to  $r_p^{2-q}$ . Dynamical lifetimes of particles are usually smaller for smaller particles, and many particles with diameter  $d \sim 1 \mu\text{m}$  are relatively quickly removed from the solar system. If we consider that a lifetime of a particle  $t_{dl} \sim d$  (at  $1 < d < 1000 \mu\text{m}$ , this assumption is in a general agreement with dynamical lifetimes of particles obtained by Ipatov and Mather 2006; destruction of particles is not considered) and  $q=3.5$ , then the brightness of migrating particles with diameter  $d$  is proportional to  $d^{-1/2}$  and the total brightness of particles with diameters between  $d_1$  and  $d_2$  is proportional to  $\sqrt{d_2} - \sqrt{d_1}$ . These our estimates are in accordance with that particles with  $d < 20 \mu\text{m}$  are not main contributors to the zodiacal light.

Dermott et al. (2001, 2002) noted that the cross-sectional area of material in the asteroid belt should be concentrated in particles with  $d \sim 1000 \mu\text{m}$  and many of these large particles are broken up by collisions before they reach a distance from the Sun  $R=1$  AU. Grün et al. (1985) considered that the Poynting-Robertson drag lifetime is comparable to the collisional lifetime for zodiacal particles greater than 100  $\mu\text{m}$ . Liou et al. (1996) and Moro-Martin and Malhotra (2002) studied collisional lifetimes of interplanetary particles destroyed by interstellar dust particles, and the sublimation temperature of particles at several distances to the Sun. They found that collisional destruction is most important for trans-Neptunian particles with  $d$  between 6 and 50  $\mu\text{m}$ .

Ground-based spectroscopic observations allow one to study Doppler shifts of scattered solar Fraunhofer lines in the zodiacal light (e.g., James 1969; Hicks et al. 1974; Fried 1978;

East and Reay 1984; Clarke 1996; Clarke et al. 1996). Analysis of these shifts thus provides an opportunity to explore velocities of interplanetary dust in the inner solar system. Reynolds et al. (2004) were the first to obtain accurate measurements of the centroid velocities and line profiles of the scattered solar Mg I  $\lambda 5184$  absorption line in the zodiacal light, both along the ecliptic equator and at high ecliptic longitudes.

The main goal of our paper is to compare the WHAM observations with our models of the zodiacal dust cloud based on our calculations of the migration of dust particles produced by different small bodies. The models for migration of dust particles and calculations of the radial velocity profile of the scattered Mg I line are discussed in Section 2. Earlier we (Ipatov et al. 2005, 2006; Ipatov and Mather 2006; Madsen et al. 2007) compared velocities corresponding to shifts of the Mg I line obtained in our models with the WHAM observations in a short form for only a few sizes of particles. Our present studies of the velocities (Section 3) are based on analysis of many data obtained for a wide range of sizes of particles and for various sources of particles. In the papers by other authors, spectroscopic observations of the zodiacal light have been compared with analytical models, but this is the first comparison of the models based numerical integrations of migration of particles with the observations. We also compare in detail the mean width of the line (the end of Section 3) and the variation of a number density with distance from the Sun  $R \leq 3$  AU (Section 5.1) obtained in our model for different sources and sizes of particles with the results of observations, study the typical eccentricities and inclinations of zodiacal particles that better fit the WHAM observations (Section 4), and discuss the fractions of asteroidal, cometary, and trans-Neptunian particles in the zodiacal cloud which better satisfy various observations (Section 5).

## 2. Model

Our studies of the Mg I line shifts (see Section 3) use the results of following the orbital evolution of about 15,000 asteroidal, cometary, and trans-Neptunian dust particles under the gravitational influence of planets, the Poynting-Robertson drag, radiation pressure, and solar wind drag. Results of some of these integrations were presented by Ipatov et al. (2004) and Ipatov and Mather (2006, 2007) (our recent papers can be found on astro-ph and on [http://www.astro.umd.edu/~sim\\$ipatov](http://www.astro.umd.edu/~sim$ipatov) or <http://www.dtm.ciw.edu/ipatov>), but other problems (mainly the probabilities of collisions of particles with the terrestrial planets) were considered. In this section we describe models used in our studies of the migration of dust particles and for calculation of the scattered line profile.

## 2.1. Sources and sizes of model particles

The initial positions and velocities of asteroidal particles (‘ast’ runs) used in our models were the same as those of the first  $N$  numbered main-belt asteroids (JDT 2452500.5), i.e., dust particles were assumed to leave the asteroids with zero relative velocity (in Section 2.2 we discuss why we can make such assumption). The initial positions and velocities of the trans-Neptunian particles (*tn* runs) were the same as those of the first  $N$  trans-Neptunian objects (TNOs) (JDT 2452600.5). These objects had semi-major axes less than 48 AU and eccentricities less than 0.35.

The initial positions and velocities of cometary particles were the same as those of Comet 2P/Encke ( $a_o \approx 2.2$  AU,  $e_o \approx 0.85$ ,  $i_o \approx 12^\circ$ ), or Comet 10P/Tempel 2 ( $a_o \approx 3.1$  AU,  $e_o \approx 0.526$ ,  $i_o \approx 12^\circ$ ), or Comet 39P/Oterma ( $a_o \approx 7.25$  AU,  $e_o \approx 0.246$ ,  $i_o \approx 2^\circ$ ), or test long-period comets ( $e_o = 0.995$  and  $q_o = a_o \cdot (1 - e_o) = 0.9$  AU or  $e_o = 0.999$  and  $q_o = 0.1$  AU,  $i_o$  varied from 0 to  $180^\circ$  in each calculation, particles produced at perihelion; these runs are denoted as *lp* runs), or test Halley-type comets ( $e_o = 0.975$ ,  $q_o = 0.5$  AU,  $i_o$  varied from 0 to  $180^\circ$  in each calculation, particles launched at perihelion; these runs are denoted as *ht* runs). The number of prograde Halley-type comets is greater than the number of retrograde Halley-type comets, but in *ht* runs we considered a uniform distribution in  $i_o$  in order to study the role of variation in  $e_o$  in comparison with *lp* runs. We considered Encke particles launched near perihelion (runs denoted as 2P), near aphelion (runs denoted as ‘2P 0.5t’), and when the comet had orbited for  $P_a/4$  after perihelion passage, where  $P_a$  is the period of the comet (runs denoted as ‘2P 0.25t’). Calculations for particles originating from Comets 10P/Tempel 2 and 39P/Oterma are denoted as 10P and 39P runs, respectively. Note that for the same initial coordinates and velocities, initial semi-major axes and eccentricities of dust particles depend on  $\beta$  and differ from those of parent bodies, but inclinations are the same (Burns et al. 1979). All orbital elements considered in the paper take this effect into account.

For cometary particles (exclusive for *lp* and *ht* runs, in which all particles launched in perihelion), the initial value of time  $\tau$  after passing perihelion was varied (Ipatov and Mather 2006) for different particles with a step  $d\tau = 1$  day or  $d\tau = 0.1$  day near the actual value of  $\tau$  for the comet (true anomaly can be considered instead of  $\tau$ ). Comet 10P/Tempel 2 is an example of a typical Jupiter-family comet moving inside Jupiter’s orbit; Comet 39P/Oterma moves outside of Jupiter’s orbit. Comet 2P/Encke is the only known high-eccentricity comet with aphelion distance  $Q < 4.2$  AU, but there could be smaller cometary objects in such orbits. Ipatov and Mather (2003, 2004a-b) obtained that some Jupiter-crossing objects can get orbits entirely located inside Jupiter’s orbit and move in such orbits for millions or even hundreds of millions of years. Probably most of such objects disintegrate during such times and produce smaller objects. Comet Encke comes close to the Sun and produces a lot of



dust (Lisse et al. 2004).

In our calculations for asteroidal and cometary particles, the values of  $\beta$ , the ratio of the Sun’s radiation pressure force to gravitational force, varied from  $\leq 0.0004$  to 0.4. Burns et al. (1979) obtained  $\beta = 0.573 Q_{pr} / (\rho s)$ , where  $\rho$  is the particle’s density in grams per cubic centimeter,  $s$  is its radius in micrometers, and  $Q_{pr}$  is the radiation pressure coefficient, which is close to unity for particles larger than  $1 \mu\text{m}$ . For silicates at density of  $2.5 \text{ g cm}^{-3}$ , the  $\beta$  values equal to 0.004, 0.01, 0.05, 0.1, and 0.4 correspond to particle diameters  $d$  of about 120, 47, 9.4, 4.7, and 1 microns, respectively. For water ice,  $d$  is greater by a factor of 2.5 than that for silicate particles. The orbital evolution of dust particles was studied by us for a wider range of masses (including particles up to several millimeters) than in most papers by other authors (e.g., Dermott et al. 2001, 2002; Gorkavyi et al. 1997, 1998, 2000a-b; Grogan et al. 2001; Kortenkamp and Dermott 1998; Liou et al. 1995, 1996, 1999; Liou and Zook 1999; Moro-Martin and Malhotra 2002, 2003; Ozernoy 2001; Reach et al. 1997). Most scientists considered particles with diameter  $d < 50 \mu\text{m}$ . Wide range of diameters was considered only by Nesvorný et al. (2006) and Kehoe et al. (2007) for asteroidal particles from the Veritas and Karin families.

## 2.2. Integration of the motion of dust particles

In our integrations we took into account the gravitational influence of planets (excluding Pluto for asteroidal and cometary particles), the Poynting-Robertson drag, radiation pressure, and solar wind drag. As Liou et al. (1999) and Moro-Martin and Malhotra (2002), we assume the ratio of solar wind drag to Poynting–Robertson drag to be 0.35. According to Grün et al. (2000), the Lorentz force is comparable to solar gravitational interaction for particles of  $d \sim 0.1 \mu\text{m}$  at 1 AU and of  $d \sim 1 \mu\text{m}$  at 50 AU from the Sun. Interstellar particles dominate among such small particles, but they are not significant contributors to the zodiacal light. Since we considered mainly larger interplanetary particles, we did not include the Lorentz force in our modeling.

Migration of dust particles was integrated using the Bulirsh-Stoer method (BULSTO) with the relative error per integration step less than  $10^{-8}$ . The BULSTO code in the SWIFT integration package (this package also includes a symplectic code) by Levison and Duncan (1994) was modified to include the additional forces of radiation pressure, Poynting-Robertson drag, and solar wind drag. The integration continued until all of the particles either collided with the Sun or drove away to 2000 AU from the Sun. For small  $\beta$ , considered time intervals exceeded 50-80 Myr (240 Myr for trans-Neptunian particles). In each calculation (with a fixed source of particles and  $\beta = \text{const}$ ) we took  $N \leq 250$  particles, because

for  $N \geq 500$  the computer time per calculation for one particle was several times greater than for  $N = 250$ . The total number of particles in several tens of runs was about 15,000. In our calculations, orbital elements were stored with a step  $d_t$  of 20 yr for asteroidal and cometary particles and 100 yr for trans-Neptunian particles during all considered time intervals. The stored orbital elements of all particles during their dynamical lifetimes were then used in our studies presented in the next sections.

The largest asteroids and TNOs do not represent accurate orbital distribution of bodies producing dust in the asteroid and trans-Neptunian belts, but for our conclusions we do not need to consider more accurate distributions than those we used. For example, for solar elongation  $60^\circ \leq \epsilon \leq 180^\circ$  at average initial eccentricity  $e_o$  of particles originating inside Jupiter's orbit equal to 0.15 and 0.5 (*ast* and 10P runs), in Section 3 we obtained the shift of spectra received at the Earth (from the solar spectrum) in the same direction (to blue). At  $e_o \geq 0.85$  the shift was in another direction. Therefore for conclusions of the present paper, the difference in  $e_o$  between 0.15 and 0.2 or between 0.4 and 0.5 is not essential. Considered parent comets show examples of comets moving inside Jupiter's orbit at two different eccentricities (0.53 and 0.85), a comet outside of Jupiter's orbit, and comets moving with  $e_o > 0.97$ . In the present paper we find general dependence of spectral shift on eccentricity. Thus for our estimates we do not need to make integrations for many different comets.

Each integration was made for a fixed size of particles. We did not study mass distribution of particles, but as it is discussed in Section 5.2, for the conclusions made in the present paper, we do not need to know accurate mass distributions of particles. Therefore we did not consider destruction of colliding particles. The destruction affects mainly lifetimes of particles and their size distributions at different distances from the Sun. It can change the distribution of the particles' orbital elements during their migration via the zodiacal cloud, but, in our opinion, these changes cannot affect the conclusions of the present paper, because these conclusions will not be changed even if real mean eccentricities in a run will differ by a factor of up to 1.5 from the values obtained for our model without destruction. Future models, which will consider the size distributions and destruction of particles, will allow one to make more accurate estimates of the fractions of zodiacal particles of different origin than those presented in the present paper.

Planets were assumed to be material points. However, using orbital elements obtained with a step  $d_t$ , Ipatov and Mather (2006, 2007) calculated the mean probability of a collision of a particle with the terrestrial planets during the particle dynamical lifetime. Later we considered the probabilities of collisions of migrating particles with the giant planets. For most calculations, the total probability  $p_{all}$  of collisions of a particle with all planets during

a dynamical lifetime of the particle was small (less than 0.01). Only for *tn* and 39P particles,  $p_{all}$  could exceed 0.01. For trans-Neptunian particles, the probabilities  $p_{jn}$  of collisions of particles with all giant planets during dynamical lifetimes of the particles were about 0.15 at  $\beta \sim 0.002-0.01$  and did not exceed 0.05 at  $\beta \geq 0.05$ . At  $\beta$  equal to 0.002, 0.01 and 0.05 for *tn* runs, the main contribution to  $p_{jn}$  ( $0.9p_{jn}$ ,  $0.5p_{jn}$ , and  $0.5p_{jn}$ ) was due to Neptune, Jupiter, and Saturn, respectively. For Comet 39P particles, the values of  $p_{all} \approx p_{jn}$  were about 0.018, 0.044, and 0.017 at  $\beta$  equal to 0.0001, 0.001, 0.01, respectively, and Jupiter’s contribution was about 85%. For particles produced by asteroids and other comets, the values of  $p_{all}$  were smaller than those for trans-Neptunian and Comet 39P particles, and the main contribution to  $p_{all}$  was due to Jupiter if particles reached Jupiter’s orbit (for some runs for all particles, aphelion distance  $Q < 5$  AU). For example, for *ht* particles we obtained  $p_{all} \approx p_{jn} \leq 0.004$ .

As  $p_{all}$  is relatively small, then even if some particles actually collide with planets, the distribution of particles over their orbital elements during their dynamical lifetimes will be practically the same as in the model for which planets are considered as material points, and the average dynamical lifetime of particles in our calculations usually will be greater than the actual value  $T_{av}$  by less than  $p_{all}T_{av}$ . The probability of a collision of a particle with Jupiter is smaller than 0.1 for trans-Neptunian particles and can be much smaller for other particles. For a small number of particles ( $N \leq 250$ ), our approach can give better estimates of the probabilities of collisions of particles with planets than direct integration of the collisions, especially in the cases when the expected number of collisions of all  $N$  particles does not exceed 1. For initial data considered, most of  $N$  particles did not collide with planets, and even if some particles in our calculations changed their eccentricities at too close encounters with planets – material points, the main contribution to variations in mean orbital elements was from particles that had not such very close encounters with planets that actually could result in collisions. Accurate values of mean eccentricities and inclinations are not needed for conclusions made in the present paper. Therefore we expect that our considered model does not change the distribution of orbital elements of particles that enter the zodiacal cloud in such a way that it can influence the conclusions of the paper.

In our calculations we considered particles leaving the parent bodies with a zero velocity. Actually such velocities have nonzero values, but it does not affect the conclusions of the present paper because relative velocities of particles produced by asteroids, TNOs, and comets are small compared to their orbital velocities and even to differences between orbital and circular velocities. Results of studies of particles ejected from Comet Tempel 1 showed (e.g., Jorda et al. 2007, Ipatov and A’Hearn 2006) that even for the collision of the Deep Impact (DI) spacecraft with the comet at a velocity of  $10 \text{ km s}^{-1}$ , relative velocities of most ejected particles did not exceed  $200-300 \text{ m s}^{-1}$ . Typical collisional velocities in the main asteroid belt are about  $5 \text{ km s}^{-1}$  (Bottke et al. 1994) and are smaller than the velocity of

the DI collision, so typical relative velocities of dust particles originating from asteroids will be smaller than  $200 \text{ m s}^{-1}$ . Gombosi et al. (1985) and Sekanina (1987) concluded that the initial velocities of particles relative to a comet are less than  $1 \text{ km s}^{-1}$ . Each our calculation was made for various parent asteroids (or TNOs), so if we will consider a nonzero distribution of relative velocities of dust particles, the final distribution of orbital elements of produced particles will be practically the same as that for a zero relative velocity.

We studied the model for which a particle collides with the Sun when perihelion distance of its orbit reached the radius of the Sun. For most considered runs, exclusive of some *lp*, *ht*, and 2P runs, for the above model, dynamical lifetimes of particles are practically the same as those for the model in which we consider direct collisions of particles with the Sun (for the latter model, a step of integration could be greater than radius of the Sun).

### 2.3. The Scattered line profile

We calculated how the solar spectrum was changed after the light had been scattered by the dust particles and observed at the Earth. This was carried out by first considering all orbital elements of dust particles during a single run, which were stored in computer memory with a step  $d_t$ . Based on these stored orbital elements, we calculated velocities and positions of particles and the Earth during the dynamical lifetimes of the particles. For each pair of positions of a particle and the Earth, we then calculated many ( $\sim 10^2$ - $10^4$ , smaller values are for larger maximum dynamical lifetimes of particles) different positions of the particle and the Earth during the period  $P_{rev}$  of revolution of the particle around the Sun, assuming that orbital elements do not vary during  $P_{rev}$ . The model, which is based on all positions and velocities of dust particles during their dynamical lifetimes, represents the zodiacal dust cloud for the case when small bodies continuously produce dust at a constant rate along their orbits. We did not consider seasonal effects and jumps in production of dust. The model considered allows one to study the main differences between spectra corresponding to particles produced by asteroids, comets, and trans-Neptunian objects.

The choice of a scattering function was based on analysis of dependences of scattering functions on angles  $\theta$  and  $\epsilon$  (see below) and wavelength presented in several papers (e.g., Giese 1963; Giese and Dziembowski 1969; Leinert 1975; Leinert et al. 1976; Weiss-Wrana 1983; Hong 1985; Lamy and Perrin 1986), which mainly followed the Mie theory for scattering. The scattering function depends on the composition of particles, their sizes, and other factors. However, we considered three simple scattering functions: (1)  $g=g_\theta=1/\theta$  for  $\theta < c_\theta$ , and  $g_\theta=1 + (\theta - c_\theta)^2$  for  $\theta \geq c_\theta$ , where  $\theta$  is the angle between the Earth and the Sun, as viewed from the particle, in radians, and  $c_\theta=2\pi/3$  radian; (2) besides the above dependence of  $g_\theta$

on  $\theta$ , the same dependence  $g_\epsilon$  on elongation  $\epsilon$  was considered ( $g=g_\theta \cdot g_\epsilon$ ), where  $\epsilon$  is the angle between the particle and the Sun, as viewed from the Earth (eastward from the Sun); (3) isotropic scattering ( $g=1$ ). For all three functions, the intensity  $I$  of light that reaches the Earth was considered to be proportional to  $\lambda^2 \cdot (R \cdot r)^{-2}$ , where  $r$  is the distance between the particle and the Earth,  $R$  is the distance between the particle and the Sun, and  $\lambda$  is the wavelength of light. Since we considered the scattering near a single spectral line, wavelength  $\lambda$  in our calculations was essentially a constant. Except for lines of sight close to the Sun, these three scattering functions give virtually the same results (see Section 3). Since the differences between the scattering functions that we considered were much greater than the differences between scattering functions presented in the publications cited above, we conclude that we need not worry about the precise form of the scattering.

For each particle position, we calculated  $r$ ,  $R$ , and projections  $v_{ps}$  and  $v_{ep}$  of velocities of particles relative to the Sun and the Earth on the lines of sight from particles to the Sun and the Earth, respectively (a projection of velocity is positive if a corresponding distance increases). These parameters and the scattering function  $g$  were then used to calculate zodiacal light spectrum (using brightness integral) as observed from the Earth. The line of sight is characterized by  $\epsilon$  and by its inclination  $i$  above the ecliptic plane. Particles along the line of sight within the beam of diameter  $2^\circ$  (Fig. 1) or  $2.5^\circ$  (other figures) were considered. In each calculation, all particles had the same size (i.e., the same  $\beta$ ), the same scattering properties, and the same source (e.g., asteroidal). The main steps of the calculation of a model spectrum are the following. For all positions and relative velocities of particles, at different values of  $\lambda$ , we calculated the intensity of light that reaches the Earth after solar light has been scattered by a particle at considered positions and velocities of the particle and the Earth. For these calculations, we considered the Doppler shift of  $\lambda$  ( $d_\lambda = \lambda(v_{ps} + v_{ep})/v_l$ , where  $v_l$  is the speed of light) and the known intensity of light vs.  $\lambda$  for the solar spectrum and supposed that the intensity of the light received at the Earth is proportional to  $g \cdot \lambda^2 / (r \cdot R)^2$ . We calculated the brightness integral using the particle distribution along the beam, provided by our model. The observations were done at one specific epoch, but the model accumulates the scattered light from particles at many different epochs. In our opinion, variations of actual spectrum with epoch usually do not exceed the differences in spectra obtained in our runs at different masses of particles and may be within the accuracy of observations. Spectra for different sources of dust considered in the present paper differed significantly (see Section 3). Therefore, if we had observations at different epochs, it would not affect conclusions of the present paper.

< Place for Figure 1 >

### 3. Variations in Solar Spectrum Caused by Scattering by Dust Particles

Figure 1 shows sample spectra of scattered Mg I  $\lambda 5184$  line obtained from our calculations toward sightlines in the antisolar direction (Fig. 1a) and toward the ecliptic pole (Fig. 1b). The spectra consist of intensity vs. wavelength shift  $\Delta\lambda$  with respect to 5183.62 Angstrom. The thinnest line in Fig. 1 denotes the initial (unscattered) solar spectrum. The plots in the figure are presented for the scattering function (2), but the lines are practically the same for three different scattering functions considered. In the figure legend, the number 0.2 or 0.05 denotes  $\beta$ , and ‘180’ in Fig. 1a denotes solar elongation  $\epsilon$  (in degrees). The WHAM observations are presented by crosses. These observations and all other plots in Fig. 1 were stretched vertically so that the minimum in the line was at approximately the same depth as that for the initial solar spectrum. The continuum levels were also normalized to 1. Similar plots at  $\epsilon=90^\circ$  and  $\epsilon=270^\circ$  for zero inclination above the ecliptic plane were presented by Ipatov et al. (2005). Unlike results by Clarke et al. (1996) and Clarke (1996) who considered spectrum near 4861 Angstrom ( $H_\beta$  line of hydrogen), our modeled spectra don’t exhibit strong asymmetry. We similarly found that minima in the plots of dependencies of the intensity of light on its wavelength near 5184 Angstrom are not as deep as those for the initial solar spectrum. Note that in the paper by Clarke et al. (1996) elongation is measured in the opposite clockwise direction than in our present paper, so our  $90^\circ$  corresponds to  $270^\circ$  in their paper.

At the North Ecliptic Pole, the calculated spectrum was shifted slightly to the left (to the blue) relative to the solar spectrum for asteroidal particles and slightly to the right (to the red) for particles originating from Comet 2P/Encke (Fig. 1b). These shifts may be due to small asymmetries in the model particle distributions with respect to the ecliptic plane. The spectra of Comet 10P and Comet 39P particles and those from long-period comets were very similar to each other. For cometary particles, the line profile has a flatter bottom than that for asteroidal particles, but it was not as wide as the observed spectrum presented by Reynolds et al. (2004). None of our model runs matched the large width of the observation toward the ecliptic pole. This issue will not be addressed in this paper, but will be a topic for future investigation and may need additional, more accurate observations.

Using the model spectrum similar to that presented in Fig. 1a, we determined the shift  $D_\lambda$  of the model spectrum with respect to the solar spectrum by comparing line centroids, for a number of lines of sight at different solar elongations  $\epsilon$ . Based on  $D_\lambda$ , we calculated ‘characteristic’ velocity  $v_c=v_l \cdot D_\lambda/\lambda$ , where  $v_l$  is the speed of light and  $\lambda$  is the mean wavelength of the line. The plot of  $v_c$  vs. the solar elongation  $\epsilon$  along the ecliptic plane is called the ‘velocity-elongation’ plot. The Doppler shift of the line centroid in the zodiacal spectrum with respect to unshifted solar line depends on many properties of the zodiacal

cloud, such as dust spatial distribution, particle sizes, velocities and their dispersion and scattering function. The resulting zodiacal light spectrum is defined by what is usually referred to in the literature as brightness integral. Inverting brightness integral and solve for the real dust particles velocities along the line of sight is not a trivial task (e.g. Schuerman 1979) and can be quite challenging. Note that  $v_c$  corresponding to the Doppler shift of the line centroid is not a velocity that can be attributed directly to some particular group of particles, but merely a compound parameter for the model verification and its comparison with the observational data. The value of  $D_\lambda$  depends on values of  $r$ ,  $R$ ,  $v_{ps}$ ,  $v_{ep}$ , and  $g$  for many dust particles. This dependence is caused by that for construction of each plot similar to that in Fig. 1a we need to consider all particles in the beam at a given solar elongation  $\epsilon$ , and for each particle we need to calculate the intensity and the Doppler shift in zodiacal light spectrum observed from the Earth. The intensity depends on  $r$ ,  $R$ , and  $g$ , and the shift depends on velocities  $v_{ps}$  and  $v_{ep}$  (see Section 2.3). For calculation of one value of  $D_\lambda$ , we need to know all values of intensity vs.  $\lambda$  (near  $\lambda=5183.62$  Angstrom) in a plot similar to Fig. 1a, to find the center of mass of the area located above the absorption line curve and under the projected level of continuum (in Fig. 1 the level is equal to 1), and to calculate the difference between the  $\lambda$  coordinate of this center of mass and that for the corresponding center of mass for the solar light. Comparison with the results of WHAM data was done in velocity shift  $v_c$  rather than in wavelength change  $D_\lambda$  making it consistent with generally accepted in studies of the zodiacal light Doppler shift. ‘Velocity-elongation’ plots are presented in Figs. 2-4. For plots marked by  $c$ , we considered the shift of the centroid (the ‘center of mass’ of the line), while ‘velocity-elongation’ curves marked by  $m$  denote the shift of the minimum of the line. ‘Velocity-elongation’ plots for different scattering functions are denoted as  $c1$  and  $m1$  for the scattering function 1, as  $c2$  and  $m2$  for the function 2, and as  $c3$  and  $m3$  for the function 3. The lines in Fig. 1 are nearly symmetric, so the results for ‘c’ and ‘m’ in Fig. 2 differ only a little. In Fig. 2 comparison of plots is presented for two runs, but similar comparison was made and similar results were obtained for other sources of particles. In Figs. 3-4 the results were obtained using only the second scattering function. The values of scattering function are large at elongation close to 0. Therefore the absolute values of velocities in Figs. 2-4 are large for small  $\epsilon$ . Velocity changes a sign at  $\epsilon=0$ .

< Place for Figures 2-4 >

‘Velocity-elongation’ curves characterize all observations along the ecliptic plane and allow one to make more reliable conclusions than the plots similar to Fig. 1. Note that plots in Fig. 1a are presented for  $\epsilon=180^\circ$ , and for other elongations the difference between the model and solar spectra can be much greater than at  $\epsilon=180^\circ$  (see Figs. 3-4). The details of the model spectra depend on  $\epsilon$ ,  $\beta$ ,  $i_\odot$ , and the source of particles. The ‘velocity-elongation’ curves obtained for different scattering functions were similar at  $30^\circ < \epsilon < 330^\circ$  (Fig. 2); though

the difference was greater for directions close to the Sun. Some not smooth parts of the curves are caused by small number statistics for these calculations. A comparison of the observed ‘velocity-elongation’ curve with those obtained from our model for dust particles of different sizes (i.e., at different values of  $\beta$ ) produced by asteroids, comets (2P/Encke, 10P/Tempel 2, 39P/Oterma, long-period, Halley-type), and trans-Neptunian objects allowed us to draw some conclusions about the sources of zodiacal dust particles. Asteroidal, trans-Neptunian, Comet 2P, and  $lp$  particles populations produce clearly distinct model spectra of the zodiacal light. The curves for  $lp$  and  $ht$  runs did not differ much from each other. The main contribution to the zodiacal light is from particles at  $\beta \sim 0.002-0.02$  (Grün et al. 1985). Therefore particular attention must be paid to the curves at such values of  $\beta$ . At  $90^\circ \leq \epsilon \leq 270^\circ$ , the projection of a velocity of a prograde particle on the direction of Earth’s velocity is usually less than the velocity of the Earth (but has the same sign) because the particles are located farther from the Sun than the Earth. The difference between the projection of a velocity of a particle on the direction of the Earth’s velocity and the Earth’s velocity has different signs at  $\epsilon=90^\circ$  and  $\epsilon=270^\circ$ . Therefore in most cases, velocities corresponding to shifts in the Mg I line are positive at  $\epsilon=90^\circ$  and negative at  $\epsilon=270^\circ$ . The differences between ‘velocity-elongation’ curves for several sources of dust reached its maximum at  $\epsilon$  between  $90^\circ$  and  $120^\circ$  (Figs. 3–4). For future observations of velocity shifts in the zodiacal spectrum, it will be important to pay particular attention to these elongations.

< Place for Table 2 >

We consider the amplitude of ‘velocity-elongation’ curves as  $v_a = (v_{\max} - v_{\min})/2$ , where  $v_{\min}$  and  $v_{\max}$  are the minimum and maximum values of velocities at  $90^\circ \leq \epsilon \leq 270^\circ$ . The observational value of  $v_a$  is about  $12 \text{ km s}^{-1}$  (if we smooth the curve). For several dust sources, the characteristic values of  $v_a$ ,  $v_{\min}$ , and  $v_{\max}$  are presented in Table 2. Mean eccentricities  $e_z$  and mean inclinations  $i_z$  at distance from the Sun  $1 \leq R \leq 3 \text{ AU}$  are also included in the table. These mean values were calculated on the basis of the orbital elements of migrating particles stored with a time step  $d_t \sim 20-100 \text{ yr}$ . Our calculations showed that the main contribution to the brightness of a dust cloud observed at the Earth is from particles located at  $R < 3 \text{ AU}$ , and for most of the runs more than a half of the brightness is due to the particles located at a distance from the Earth  $r \leq 1 \text{ AU}$ . Thus, since only positions of particles at  $R \geq 1 \text{ AU}$  are used for calculation of the brightness of particles at elongation  $90^\circ \leq \epsilon \leq 270^\circ$ , if it is not mentioned specially, the mean eccentricities  $e_z$  and orbital inclinations  $i_z$  refer to  $1 \leq R \leq 3 \text{ AU}$ . Particular attention was paid to eccentricities and inclinations at  $1 \leq R \leq 2 \text{ AU}$ .

For asteroidal dust, the ‘velocity-elongation’ curves had lower amplitudes than the observations (Fig. 3a-b). The plots obtained at different  $\beta$  differed little from each other, especially at  $\beta < 0.01$ . For Comet 10P particles, the ‘velocity-elongation’ amplitudes were



also lower than that for the observations (Fig. 3c-d). The difference between the curves obtained for Comet 10P particles at different  $\beta$  was greater than that for asteroidal particles, but was usually less than that for other sources of particles considered. On the other hand, the ‘velocity-elongation’ curve corresponding to particles produced by Comet 2P/Encke have slightly larger amplitudes than the observational curve (Fig. 4a-b). The velocity amplitudes  $v_a$  for particles originating from long-period and Halley-type comets are much greater than those for the observational curve (Fig. 4f). Therefore perhaps a combination of Comet 2P (and/or  $lp$  and  $ht$ ) dust particles and asteroidal (and/or Comet 10P) particles could provide a result that is close to the observational ‘velocity-elongation’ curve.

The orbit of Comet 39P/Oterma is located outside of Jupiter’s orbit, but inside Saturn’s orbit. Studies of the migration of Comet 39P particles thus give some information about the migration of particles originating beyond Neptune’s orbit that have reached 7 AU from the Sun. For Comet 39P particles and  $0.01 \leq \beta \leq 0.2$  at  $60^\circ < \epsilon < 150^\circ$ , ‘velocity-elongation’ amplitudes were smaller than the observed amplitudes (Fig. 4c), while for  $\beta \leq 0.004$ , the curves more closely match the observations (Fig. 4d). For such small  $\beta$ , only a small number of particles entered inside Jupiter’s orbit, and statistics were poor. The distribution of particles over their orbital elements could be somewhat different if we had considered a greater number  $N$  of particles in one run, but the difference between the curves obtained at different  $N$  will not be more than the difference between the curves obtained at adjacent values of  $\beta$  presented in the figure. At  $\beta=0.0001$ , Comet 39P particles spent on average more time in the zodiacal cloud than at other  $\beta$ , but it was due mainly only to one particle, which during about 9 Myr moved inside Jupiter’s orbit before its collision with the Sun. In reality such particle could sublimate or be destroyed in collisions during its dynamical lifetime. Small number statistics may also be responsible for the spread of results for  $tn$  runs in Fig. 4e, as only a few trans-Neptunian particles in each run (at fixed  $\beta$ ) entered inside Jupiter’s orbit. If there had been a greater number of particles in the  $tn$  runs, the differences between the corresponding plots would probably have been smaller.

‘Velocity–elongation’ curves for asteroidal and Comet 10P particles are located below the observational curve, and those for Comet 2P particles are located above the observational curve (Figs. 3-4). Therefore a combination of different sources of particles could give a zero vertical shift. For trans-Neptunian particles, velocity amplitudes  $v_a$  were greater than the observational values at  $\beta \geq 0.05$  and were about the same at  $\beta=0.01$  (Fig. 4e). Therefore together with high-eccentricity cometary particles, trans-Neptunian particles can compensate small values of  $v_a$  for asteroidal and Comet 10P particles. The observational curve was mainly inside the region covered by trans-Neptunian curves obtained for different  $\beta$  (and by Comet 39P curves at  $\beta \leq 0.004$ ), but at  $180^\circ < \epsilon < 270^\circ$  it was mainly above the trans-Neptunian curves.

Observations by Reynolds et al. (2004) also provided the FWHM (full width at half maximum, i.e., the  $x$ -width at  $y=(y_{\min}+y_{\max})/2$ ) of the Mg I line in the zodiacal light. As Reynolds et al., we consider FWHM in  $\text{km s}^{-1}$ . The relation between the width  $\Delta\lambda_w$  of the spectrum line and a corresponding velocity  $v_w$  is the following:  $\Delta\lambda_w/\lambda = v_w/v_l$ , where  $v_l$  is the speed of light and  $\lambda$  is the mean wave length of the line. The values of  $v_w$  obtained at observations varied from 65.6 to 87.2  $\text{km s}^{-1}$ , and most of them were between 70 and 80  $\text{km s}^{-1}$ , with a mean value of 76.6  $\text{km s}^{-1}$ . For close values of  $\epsilon$ , observational values of  $v_w$  can differ considerably, e.g.,  $v_w$  equaled 65.6 and 83.9  $\text{km s}^{-1}$  at  $\epsilon$  equaled to  $179.3^\circ$  and  $174.2^\circ$ , respectively. Most of the values of FWHM obtained in our models (exclusive for 2P runs) are inside the range of observational values (see astro-ph/0608141). At  $\beta \leq 0.004$  for particles originating from Comet 2P/Encke, the width is greater at  $\epsilon \approx 220^\circ$  than at  $\epsilon \approx 45^\circ$ . Such dependence of FWHM on  $\epsilon$  is not consistent with the observations, and therefore the contribution of particles similar to Comet 2P particles to the zodiacal light cannot be considerable. For other sources of dust at  $\beta \leq 0.02$ , the width is approximately independent of  $\epsilon$  at  $30^\circ < \epsilon < 330^\circ$ . For all considered sources of dust and diameters of particles, the widths become relatively large at  $-15^\circ < \epsilon < 15^\circ$ , where there are no observations.

< Place for Figure 5 >

As the observational values of FWHM differed much at close  $\epsilon$  and may be due to observational uncertainty, it is better to compare our models with the mean value of FWHM obtained by observations. For particles originated from asteroids, Comets 2P/Encke, 10P/Tempel 2, and 39P/Oterma, and test long-period comets, the mean (at  $30^\circ < \epsilon < 330^\circ$ ) values of FWHM are mainly about 74-76, 81-88, 76-77, 76-77, 73-86  $\text{km s}^{-1}$ , respectively (the range is for various  $\beta$ ). For Comet 10P and Comet 39P particles, the mean width is slightly greater for smaller  $\beta$  at  $0.0001 \leq \beta \leq 0.1$  (Fig. 5). For Comet 2P particles, the mean values of FWHM depend on  $\beta$  and the place of origin from the orbit (i.e., the initial value of true anomaly). For 2P particles originated at perihelion, mean values of FWHM were greater than observational 76.6  $\text{km s}^{-1}$ . The mean values of FWHM obtained for particles originated from test long-period comets can differ considerably in different runs with different  $\beta$ . For  $lp$  particles, the mean width usually is even less than that for Comet 2P particles at the same  $\beta$ . At  $\beta \leq 0.01$  for  $ht$  particles, the mean width was large ( $\approx 90 \text{ km s}^{-1}$ ).

As it is summarized in Fig. 5, the mean value of FWHM for asteroidal dust at  $\beta \geq 0.0004$  is less than the 77  $\text{km s}^{-1}$  FWHM of the observations. To fit the observations of the mean width for a combination of asteroidal and cometary dust, we need to consider a greater (>50%) fraction of Comet 10P and Comet 39P particles or a smaller (<50%) fraction of Comet 2P or  $ht$  particles in the overall dust, as points for Comet 2P and  $ht$  particles at  $\beta \leq 0.02$  are located in Fig. 5 farther from the observational value than those for asteroidal

particles.

#### 4. Eccentricities and Inclinations of Zodiacal Dust Particles that Fit the Doppler Shift of Mg I Line

In order to understand the variations in the model line profiles with the source and size of particles, we examined the values of mean eccentricities and mean orbital inclinations of zodiacal dust particles. Analysis of the correlation between the values of mean eccentricities and inclinations and the values of the velocity amplitudes of ‘velocity-elongation’ plots showed that, in general, these amplitudes are greater for greater mean eccentricities and inclinations, but they depend also on distributions of particles over their orbital elements.

< Place for Figures 6-7 >

The values of  $e_z$ ,  $i_z$ ,  $v_a$ ,  $v_{\min}$ , and  $v_{\max}$  (see designations in Section 3) for particles from different sources are presented in Table 2 at several values of  $\beta$ . Analysis of this table and Figs. 3-4, 6-7 shows that at  $e_z < 0.5$  for particles originated inside Jupiter’s orbit (e.g., for particles produced by asteroids and Comet 10P), the velocity amplitudes  $v_a$  are usually smaller than the observed amplitude ( $12 \text{ km s}^{-1}$ ), while for most of runs at  $e_z > 0.5$  (e.g., for 2P and  $lp$  runs),  $v_a$  is greater than the observed amplitude. For these data, the WHAM observations correspond to a mean orbital eccentricity  $e_z$  of about 0.5. However, the velocity amplitudes of the line depend not only on  $e_z$ , but also on the distribution of all orbital elements of dust particles. For particles migrated from outside of Jupiter’s orbit ( $tn$  and 39P runs), the mean eccentricities that satisfy the WHAM observations can be  $\sim 0.1$ - $0.4$ . For example, at  $\beta = 0.004$  for 39P run, the data in Figs. 4d and 5 were not far from the observations, but mean eccentricities at  $1 \leq R \leq 2$  AU were about 0.35. On the other side, 39P runs with  $e_z \sim 0.6$ - $0.7$  also fit the WHAM observations, but such large particles ( $\beta \leq 0.001$ ) may not be dominant in the brightness. For  $tn$  runs at  $\beta \geq 0.05$ , mean eccentricities at  $1 \leq R \leq 2$  AU were even between 0.1 and 0.3 (between 0.2 and 0.4 at  $2 \leq R \leq 3$  AU), but, as it is discussed in Section 5, such particles do not dominate in the zodiacal light. For  $tn$  runs at  $\beta \leq 0.01$ , only a few particles entered inside Jupiter’s orbit, and therefore it is difficult to make any reliable conclusion. To summarize, we can conclude that for an abstract model of identical zodiacal particles from the same source, the mean eccentricities of zodiacal particles are between 0.3 and 0.5, and they are closer to 0.5 if most of the particles originated inside Jupiter’s orbit. Actually particles of different sources and sizes contribute to the zodiacal light. For example (see Section 5 for discussion of fractions of particles of different origin), for the model of the zodiacal cloud consisted of 40% of *ast* particles with  $e_z \approx 0.1$ , 40% of Comet 10P, Comet 39P, and  $tn$  particles with  $e_z \approx 0.35$ , and 20% of Comet 2P,  $lp$ , and  $ht$  particles with  $e_z \approx 0.7$  (for

particles originated from high-eccentricity comets,  $e_z$  is smaller than initial eccentricities), the mean eccentricity at  $R \sim 1-2$  AU will be about 0.3. More massive particles, exclusive for those with diameter of not more than a few microns, usually have more eccentric orbits.

In most calculations, mean eccentricities of particles decrease with  $R < 1$  AU becoming close to 0 near the Sun, and at  $R < 1$  AU the difference in mean eccentricities for particles of different origin is smaller than at  $R > 1$  AU. Therefore ‘velocity-elongation’ curves corresponding to different runs presented in Figs. 3-4 become more close to each other when  $\epsilon$  becomes more close to the direction to the Sun.

The velocity amplitudes  $v_a$  also depend on inclinations because particles in high inclination orbits have smaller projections of their orbital velocities on the lines of sight from the Earth and the Sun than particles in orbits located near the ecliptic plane. The differences between these projections and the Earth’s velocity are greater than those for small inclinations, and a vertical component of a relative velocity is greater for greater  $i$ . Mean inclinations of particles in the calculations that fit the WHAM observations do not exceed  $25^\circ$ . For 39P and  $tn$  runs, they mainly exceed  $10^\circ$ . For other runs usually  $i_z > 5^\circ$ . For  $lp$  and  $ht$  particles, the values of  $v_a$  are significantly greater than those for dust particles from other sources, and the values of  $i_z$  are much greater than for other runs. Note that mean initial inclinations for  $lp$  and  $ht$  runs are about  $90^\circ$  (initial orbital inclinations are distributed uniformly between 0 and  $180^\circ$ ), but the mean inclinations of migrating particles in some runs are mainly greater (and in other runs are mainly smaller) than  $90^\circ$  (see Fig. 7f).

The distribution of orbital parameters and the resulting scattered line profile is dependent upon  $\beta$  because  $\beta$  influences the lifetime of the particle. Dynamical lifetimes of particles are greater for smaller  $\beta$ . For Comet 2P/Encke particles with very short ( $\leq 5$  Kyr) dynamical lifetimes (e.g., for ‘2P 0.25t’ run at  $\beta=0.05$  and for ‘2P 0.5t’ runs at  $\beta=0.2$  and  $\beta=0.1$ ), ‘velocity-elongation’ curves were shifted in the velocity direction for up to  $25 \text{ km s}^{-1}$  from the observational curve and from the curves for larger ( $> 50$  Kyr) dynamical lifetimes (e.g., for ‘2P 0.25t’ runs at  $\beta=0.01$  and for ‘2P 0.5t’ runs at  $\beta=0.05$  and  $\beta=0.01$ ). Such shift can be explained based on studies of plots of eccentricities versus semi-major axes. At smaller  $\beta$ , particles migrate more slowly into the Sun and interact with planets for a longer time than for larger  $\beta$ , and therefore they exhibit a wider range of eccentricities, even though they have the same origin. ‘Velocity-elongation’ and ‘eccentricity-semi-major axis’ plots for such runs are presented in astro-ph/0608141. As the motion is stochastic and the number of particles in our runs is not large, there may be no strict dependence on  $\beta$ . At  $\beta \geq 0.1$ , ‘velocity-elongation’ curves for ‘2P 0.25t’ and ‘2P 0.5t’ runs are higher than the observational line. In this case, all eccentricities are large at  $a > 1$  AU, plots of  $a$  versus  $e$  are practically the same for all particles, and dynamical lifetimes of all particles are close to each other and are

very short ( $<5$  Kyr). For  $\beta=0.05$ , the maximum dynamical lifetime of Comet 2P particles launched at aphelion (‘2P 0.5t’ run) was greater by a factor of 4 than that for ‘2P 0.25t’ run. Therefore at  $\beta=0.05$ , the scatter of values of  $e$  at the same  $a$  was greater for ‘2P 0.5t’ run than for ‘2P 0.25t’ run. For many particles other than Comet 2P particles, dynamical lifetimes are several tens or several hundreds of thousands of years and can reach tens of millions of years (Ipatov and Mather 2006). Besides, more particles were produced by Comet 2P in its perihelion (in this case, the plots do not differ much from the observational plot even at large  $\beta$ ) than in aphelion. Therefore the zodiacal light contribution is very small for particles with  $\beta \geq 0.05$  produced by Comet 2P at aphelion or in the middle of the orbit.

## 5. Sources of Zodiacal Dust Particles

### 5.1. Our estimates based on observations used in previous studies

In this subsection we show that some observations used in the previous publications for estimates of the fraction of cometary particles in the zodiacal cloud does not contradict to the values of the fraction greater than those presented in Table 1. Based on these observations and results of our calculations, we also study fractions for other dust sources.

*Number density at  $R > 3$  AU.* First we consider the fractions that fit the observations of the number density  $n(R)$ . For particles originating inside Jupiter’s orbit,  $n(R)$  decreases quickly with distance  $R$  from the Sun at  $R > 3$  AU (Ipatov and Mather 2006). For 39P runs and  $\beta \geq 0.002$ ,  $n(R)$  was greater at  $R=3$  AU than at  $R \sim 5-10$  AU, and it was greater for smaller  $R$  at  $R < 3$  AU. Therefore the fraction of particles originating beyond Jupiter’s orbit among overall particles at  $R=3$  AU can be considerable (and even dominant) in order to fit *Pioneer’s* 10 and 11 observations, which showed (Hummes 1980; Grün 1994) that  $n(R) \approx \text{const}$  at  $R \sim 3-18$  AU and masses  $\sim 10^{-9}-10^{-8}$  g ( $d \sim 10$   $\mu\text{m}$  and  $\beta \sim 0.05$ ). Otherwise one must explain why particles migrated from 7 to 3 AU disappear somewhere. A considerable fraction of the particles originating beyond Jupiter’s orbit is also in agreement with our studies of the Doppler shift of Mg I line (Section 5.2) and the below studies of the distribution of number density between 1 and 3 AU. The number density of trans-Neptunian particles at  $R \sim 5-10$  AU is smaller by a factor of several than that at  $R \sim 20-45$  AU. Therefore in order to fit  $n(R) \approx \text{const}$ , the fraction of trans-Neptunian particles at  $R \sim 5-10$  AU must be smaller by a factor of several than the fraction of particles produced by comets at such  $R$ , and we can expect that at  $d \sim 10$   $\mu\text{m}$  the fraction of trans-Neptunian dust among zodiacal particles is smaller by a factor of several than the fraction of cometary particles originated beyond Jupiter’s orbit and probably doesn’t exceed 0.1. We also consider that the fraction of trans-Neptunian particles colliding with the Earth is probably greater than the estimate (0.01-0.02)

by Moro-Martin and Malhotra (2003).

< Place for Figure 8 >

*Number density at  $R < 3$  AU.* In Fig. 8a-c we present the values of  $\alpha$  in  $n(R) \propto R^{-\alpha}$  for  $R$  equal to 0.3 and 1 AU (a), at  $R=0.8$  and  $R=1.2$  AU (b), and at  $R$  equal to 1 and 3 AU (c). Collisions can shorten lifetimes of particles and change the distributions of particles over  $\beta$  and orbital elements, but we do not think that for the considered range of distances between 0.3 and 3 AU, collisions cause variations of  $\alpha$  greater than the differences between values of  $\alpha$  obtained at close values of  $\beta$  (see also discussion of the role of collisions in Section 5.2). Below in this section we compare the values of  $\alpha$  presented in Fig. 8 with the values of  $\alpha$  deduced from observations of the actual zodiacal cloud. The micrometeoroid flux ( $10^{-12}$  g -  $10^{-9}$  g, i.e., at  $d < 5 \mu\text{m}$  for  $\rho = 2.5 \text{ g cm}^{-3}$ , or at  $\beta \geq 0.1$ ) measured on board *Helios 1* during 1975 is compatible with  $n(R) \propto R^{-1.3}$  at  $R$  between 0.3 and 1 AU (Grün et al. 1977; Leinert et al. 1981). Observations by Earth’s satellite *IRAS* yielded  $n(R) \propto R^{-1.1}$  (Reach 1991). *Pioneer 10* observations between the Earth’s orbit and the asteroid belt yielded  $n(R) \propto R^{-1.5}$  for particles of mass  $\sim 10^{-9}$  g (Hanner et al. 1976; Reach 1992). Based on integrations of the motion of 1-5  $\mu\text{m}$  particles, at  $0.5 \leq R \leq 1.5$  AU Ozernoy (2001) obtained that  $\alpha = 1.5-1.7$  for the cometary dust,  $\alpha = 1.4$  for the trans-Neptunian dust, and  $\alpha = 1.0$  for the asteroidal dust.

In our models at  $0.3 \leq R \leq 1$  AU and  $0.001 \leq \beta \leq 0.2$ , all values of  $\alpha$  exceed 1.9 for Comet 2P particles and are smaller than 1.1 for asteroidal particles (Fig. 8a). At  $\beta \geq 0.02$ , the values of  $\alpha$  for particles originating from other considered comets were less than 1.5, but were mainly greater than those for asteroidal particles and in some runs exceeded 1.3. For two-component dust cloud model,  $\alpha = 1.3$  can be produced if we consider 86% of particles with  $\alpha = 1.1$  and 14% of particles with  $\alpha = 2$ . It means that the fraction of Comet 2P particles needed to fit the *Helios* observations is probably less than 0.15. Let us use other data to estimate this fraction. Dynamical lifetimes are different for particles of different sizes and different origin. The mean value of dynamical lifetimes of 100  $\mu\text{m}$  asteroidal and Comet 10P particles is about 0.5 Myr (Ipatov 2006). According to Fixsen and Dwek (2002), the total mass of the zodiacal cloud is  $(2-11) \cdot 10^{15}$  kg. Using the above assumptions, we obtain the influx of zodiacal dust to be about 1300-7000  $\text{kg s}^{-1}$ , though this is quite crude estimate. Lisse et al. (2004) obtained that the dust mass loss rate was between 70-280  $\text{kg s}^{-1}$  for Comet 2P/Encke at  $R = 1.17$  AU. If we take the mean values for the above two intervals, we obtain the fraction of Comet 2P/Encke particles among overall zodiacal particles to be about 0.04. The production of dust by Comet 2P/Encke at perihelion (at 0.33 AU) is greater than that at 1.17 AU. Smaller bodies moving in Encke-type orbits also produce dust. Therefore the fraction of particles similar to Comet 2P particles can exceed 0.1. Dynamical lifetimes of *lp* and *ht* particles are small at  $\beta > 0.02$ , and so the fraction of such particles in the overall

population is small at  $d < 20 \mu\text{m}$ . Observations of the number density were made for small particles, and they doesn't allow one to make conclusions on the fractions of  $lp$  or  $ht$  particles at  $\beta \leq 0.01$ .

At  $\beta \geq 0.1$  and  $0.8 \leq R \leq 1.2$  AU, the mean value of  $\alpha$  for all points in Fig. 8b was a little smaller than 1.5. For cometary dust,  $\alpha$  was mainly greater than for asteroidal dust; this difference was greater at  $\beta \leq 0.05$  than at  $\beta \geq 0.1$ . For  $\beta \leq 0.2$ , the values of  $\alpha$  for Comet 2P particles were greater than for other sources of dust considered. At  $1 \leq R \leq 3$  AU for most of the dust sources, the values of  $\alpha$  were mainly greater than the observed value equal to 1.5 (Fig. 8c). At  $0.1 \leq \beta \leq 0.2$ , the values of  $\alpha$  for particles originating from trans-Neptunian objects and Comet 39P/Oterma better fit the observational value of 1.5 than those for particles from other sources (including asteroidal dust). This is another argument that fraction of particles produced outside of Jupiter's orbit can be considerable.

Based on the above conclusion that a considerable fraction of particles originated outside of Jupiter's orbit, we can infer that dust production rate of external Jupiter-family comets could be greater than the estimate by Landgraf et al. (2002). If we use their estimate that the dust production rate of external Jupiter-family comets is  $80 \text{ kg s}^{-1} \approx 2.5 \cdot 10^9 \text{ kg yr}^{-1}$  and Grün's et al. (1985) estimate that the total dust influx to the Earth is  $\sim 3 \cdot 10^7 \text{ kg yr}^{-1}$ , then, considering that the probability of collisions of Comet 39P particles with the Earth is  $\sim 10^{-4}$  (Ipatov and Mather 2006, 2007), we obtain that the fraction of particles produced by external Jupiter-family comets among particles collided with the Earth does not exceed a few percent. Dust can be produced not only by evaporation and collisions, but also at close encounters of comets (e.g., Comet Shoemaker-Levy 9) with Jupiter. It is possible that such encounters can considerably enhance the production of dust at  $R \sim 5\text{-}10$  AU.

*Shape of microcraters.* In our opinion, the shape (diameter/depth ratio) of microcraters does not contradict to values of the fraction of asteroidal dust smaller than those obtained by Brownlee et al. (1973), Vedder and Mandeville (1974), Nagel and Fechtig (1980), and Fechtig et al. (2001). The above authors concluded that about 30% of the dust particles impacting upon the Lunar surface indicate material densities of  $< 1 \text{ g cm}^{-3}$  and therefore more than 70% of interplanetary particles at  $R=1$  AU are of asteroidal origin. We consider that not all cometary particles have such small densities because comets also include more dense material. Cometary particles have greater eccentricities and inclinations at  $R=1$  AU and therefore greater velocities relative to the Moon than asteroidal particles. Hence the probability to be captured by the Moon (or the Earth) is greater for a typical asteroidal particle than for a typical cometary particle. For high-eccentricity cometary particles, these probabilities can be less than those for asteroidal particles by 2 to 4 orders of magnitude (Ipatov and Mather 2006). The ratio of the fraction of particles accreted by the Earth

to the fraction of particles in the zodiacal cloud is different for different parent bodies. This difference was discussed by several authors (e.g., Nesvorný et al. 2006). Note that probabilities of collisions of particles with a celestial body depend mainly not on mean values of eccentricity and inclination, but on the fraction of particles with small  $e$  and  $i$ . Therefore the difference in the probabilities can be much greater than the difference in mean eccentricities. To summarize the above, we conclude that less than 70% (e.g., 30-50%) of asteroidal particles can also fit the observations of the crater shape.

*Shape of the zodiacal cloud.* For our  $tn$  runs,  $i_z$  was greater than for  $ast$ , 2P, and 10P runs, it was about the same as for 39P runs, and it was much smaller than for  $lp$  and  $ht$  runs. Our studies of  $i_z$  indicate that it may be possible to find such combinations of fractions of particles originating from different comets that fit the observations of brightness vs. latitude even without trans-Neptunian particles. Therefore both 1/3 (suggested by Gorkavyi et al. 2000a and Ozernoy 2001) and even 0 for the fraction of trans-Neptunian particles can fit the *COBE* observations of brightness vs. latitude. In our runs at all  $R$ , including  $R < 1$  AU, the characteristic inclinations  $i_c$  of particles originating from Jupiter-family comets were often greater than  $7^\circ$ , and  $i_c > 7^\circ$  for some sizes of asteroidal particles (Fig. 7). Therefore the fraction of particles produced by asteroids and Jupiter-family comets among the optical dust cross-section seen in the ecliptic at 1 AU that fit the *Clementine* observations inside the orbit of Venus can be greater than the value of 45% obtained by Hahn et al. (2002). Hahn et al. considered three sources: dust from asteroids and Jupiter-family comets with the characteristic inclination of about  $7^\circ$ , dust from Halley-type comets having  $i \sim 33^\circ$ , and an isotopic cloud of dust from Oort Cloud comets.

## 5.2. Estimates based on the WHAM observations

Comparison of the ‘velocity-elongation’ plots and of the mean width of the Mg I line obtained at the WHAM observations with the plots and the width based on our models provide evidence of a considerable fraction of cometary particles in zodiacal dust, but it does not contradict  $>30\%$  of asteroidal dust needed to explain formation of dust bands. In the future we plan to explore the fractions of particles of different origin in the overall dust population based on various observations and taking into account a model for the size distribution of particles. Here we present estimates based on a much simpler, two-component zodiacal dust cloud that fits the observations of a velocity amplitude  $v_a$ . For example, with  $v_a = 9 \text{ km s}^{-1}$  for asteroidal dust (or Comet 10P particles) and at  $v_a = 14 \text{ km s}^{-1}$  for Comet 2P particles, the fraction  $f_{ast10P}$  of asteroidal dust plus cometary particles similar to Comet 10P particles would have to be 0.4. If all of the high-eccentricity cometary particles in the



zodiacal cloud were from long-period comets ( $v_a=33 \text{ km s}^{-1}$ ), then  $f_{ast10P}=0.88$ . Therefore for the above two-component models, we have  $f_{ast10P}\sim 0.4-0.9$ , with  $1-f_{ast10P}$  of brightness of the zodiacal cloud due to particles produced by high-eccentricity ( $e>0.8$ ) comets. The contribution of  $lp$  particles to the zodiacal light cannot be large because their inclinations are large and *IRAS* observations showed (Liou et al. 1995) that most of the zodiacal light is due to particles with inclinations  $i<30^\circ$ . Also  $lp$  and  $ht$  particles alone cannot provide constant number density at  $R\sim 3-18 \text{ AU}$ . At  $\beta\geq 0.004$ ,  $lp$  particles are quickly ejected from the solar system, so, as a rule, among zodiacal dust we can find  $lp$  particles only with  $d>100 \mu\text{m}$ . The contribution of  $lp$  particles to the total mass of the zodiacal cloud is greater than their contribution to the brightness  $I$ , as surface area of a particle of diameter  $d$  is proportional to  $d^2$ , and its mass  $M\propto d^3$ , i.e.,  $M/I\propto d$ . Comet 2P,  $lp$ , and  $ht$  particles are needed to compensate for the small values of  $v_a$  ( $\sim 8-9 \text{ km s}^{-1}$ ) for asteroidal and Comet 10P particles. Formally, the observed values of  $v_a$  can be explained only by Comet 39P and trans-Neptunian particles, without any other particles (including asteroidal particles). Cometary particles originating beyond Jupiter's orbit are needed to explain the observed number density at  $R>5 \text{ AU}$ , so the contribution of such particles to the zodiacal light is not small. Therefore the values of  $f_{ast10P}$  can be smaller than those for the two-component models discussed above, but the contribution of  $lp$  and  $ht$  particles (with  $e_o\geq 0.975$ ) to the zodiacal light cannot exceed 0.1 in order to fit the observations of  $v_a$ .

The dynamical lifetimes of  $lp$  particles at  $\beta\leq 0.002$  (i.e., at  $d>200 \mu\text{m}$ ) can exceed several Myrs (i.e., can exceed mean lifetimes of asteroidal and Comet 2P particles). Thus the fraction of large  $lp$  particles in the zodiacal cloud can be greater than their fraction in the new particles that were produced by small bodies or came from other regions of the solar system. Dynamical lifetimes of dust particles are usually greater for greater  $d$  (Ipatov and Mather 2006), and some particles can be destroyed by collisions with other particles. Therefore the mass distributions of particles produced by small bodies are different from the mass distributions of particles located at different distances from the Sun.

Our studies presented above do not contradict to the model of the zodiacal cloud for which fractions of asteroidal particles, particles originating beyond Jupiter's orbit (including trans-Neptunian particles), and cometary particles originating inside Jupiter's orbit are about 1/3 each, with a possible deviation from 1/3 up to 0.1-0.2. As it is discussed in Introduction and Section 5.1, a considerable fraction of cometary particles among zodiacal dust is in accordance with most of other observations. Our estimated fraction of particles produced by long-period and Halley-type comets in zodiacal dust does not exceed 0.1-0.15. The same conclusion can be made for particles originating from Encke-type comets (with  $e\sim 0.8-0.9$ ).

Though our computer model is limited, the main conclusions on the fractions of particles

of different origin among zodiacal dust are valid for a wider range of models. Each ‘velocity-elongation’ curve used in our present studies of fractional contributions was obtained for a fixed size of particles. Our calculations showed that the difference between characteristic velocities corresponding to shifts in the Mg I line (or between mean eccentricities) for different sizes of particles was usually less than the difference for different sources of particles (e.g., asteroidal, Comet 2P, and Comet 39P particles). It means that reasonable variations of mass distributions of zodiacal particles do not influence on our conclusions about the fractions of asteroidal and cometary dust among overall zodiacal particles. Eccentricities and inclinations of most zodiacal particles are not small and their mean values usually do not differ much for different relatively close values of  $\beta$  (see Figs. 6-7). We expect that mean variations in orbital elements of the particles due to collisions are smaller than these elements and these variations do not change our conclusions about sources of zodiacal particles. The collisional lifetimes of particles may be comparable or shorter than their dynamical lifetimes, and production of different particles can be different at different distances from the Sun. For more accurate models, collisional processes must be taken into account, but the conclusions made in the present paper do not depend on collisional evolution of particles. In our simulations of spectra of dust particles we did not take into account that albedo can be different for particles of different origin. Mean albedo of cometary particles is smaller than that of asteroidal particles and interplanetary dust (typical albedo is  $0.1 \pm 0.05$  for interplanetary dust, 0.02-0.06 for comets,  $0.14 \pm 0.1$  for TNOs, 0.03-0.09, 0.1-0.18, 0.1-0.22, and  $>0.3$  for C-type, M-type, S-type, and E-type asteroids, respectively; see Hahn et al. 2002, Fernandez et al. 2005, Grundy et al. 2005). Therefore the fraction of cometary particles among overall particles will be greater than their contribution to the zodiacal light, and our conclusion about a considerable fraction of cometary dust will be only enhanced.

There is no considerable difference in the ratio of fractions of asteroidal/cometary/trans-Neptunian dust for our spectroscopic studies at different  $\epsilon$ , as our studies showed that the main contribution to the spectrum is from particles at a distance less than 1 AU from the Earth and similar vertical shifts of the ‘velocity-elongation’ curves (different for different sources of dust) from the observational curve were obtained for many values of  $\epsilon$  (see Figs. 3-4). Considerable difference in the fractions at different  $\epsilon$  may occur if we consider particles in different parts of the solar system, separated by several AU. In the future we plan to consider mass distributions of particles. The contribution of particles of different sizes can depend on  $\epsilon$  (but not considerably). It is caused, for example, by the result that more massive particles spend more time in the near-Earth ring (Ipatov et al. 2004). Therefore the size distribution of particles at  $\epsilon$  close to  $90^\circ$  and  $270^\circ$  can differ from that for other values of  $\epsilon$ .

## 6. Conclusions

Our study of velocities corresponding to Doppler shifts and widths of the Mg I line in the zodiacal light is based on the distributions of positions and velocities of migrating dust particles originating from various solar system sources. These distributions were obtained from our integrations of the orbital evolution of particles produced by asteroids, comets, and trans-Neptunian objects. At the elongations of the fields observed by WHAM, the model curves of the characteristic velocity of the line vs. the solar elongation (‘velocity-elongation’ curves) were close to each other for several scattering functions considered. The differences between the curves for several sources of dust reached its maximum at elongation between  $90^\circ$  and  $120^\circ$ . Therefore it is important for the future zodiacal light Doppler shifts measurements to pay a particular attention to observing at this elongation range, since this is the elongation range that allows to have the best discrimination between the different dust sources.

The comparison of ‘velocity-elongation’ curves and the line width averaged over the elongations obtained at observations made by Reynolds et al. (2004) with the corresponding curves and mean widths obtained in our models shows that asteroidal dust particles alone cannot explain these observations, and that particles produced by comets, including high-eccentricity comets (such as Comet 2P/Encke and long-period comets), are needed. The conclusion that a considerable fraction of zodiacal dust is cometary particles is also supported by the comparison of the variations of a number density with a distance from the Sun obtained in our models with the spacecraft observations. Cometary particles originating inside Jupiter’s orbit and particles produced beyond Jupiter’s orbit (including trans-Neptunian dust particles) can contribute to zodiacal dust about  $1/3$  each, with a possible deviation from  $1/3$  up to 0.1-0.2. The fraction of asteroidal dust is estimated to be  $\sim 0.3-0.5$ . The estimated contribution of particles produced by long-period and Halley-type comets to zodiacal dust does not exceed 0.1-0.15. The same conclusion can be made for particles originating from Encke-type comets (with  $e \sim 0.8-0.9$ ).

The velocity amplitudes of ‘velocity-elongation’ curves are greater for greater mean eccentricities and inclinations, but they depend also on distributions of particles over their orbital elements. The mean eccentricities of zodiacal particles located at 1-2 AU from the Sun that better fit the WHAM observations are between 0.2 and 0.5, with a more probable value of about 0.3.

## Acknowledgements

This work was supported by NASA (NAG5-12265) and by the National Science Foundation through AST-0204973. We are thankful to David Nesvorný and another reviewer for helpful discussion.

## REFERENCES

- Bottke, W. F., Nolan, M. C., Greenberg, R., Kolvoord, R. A. 1994. Velocity distributions among colliding asteroids. *Icarus* **107**, 255-268.
- Brownlee, D. E., Joswiak, D. J., Love, S. G., Nier, A. O., Schlutter, D. J., and Bradley, J. P. 1993. Identification of cometary and asteroidal particles in stratospheric IDP collections. *Lunar Planet. Sci.* **24**, 205-206.
- Burns, J. A., Lamy, P. L., and Soter, S. 1979. Radiation forces on small particles in the Solar System. *Icarus* **40**, 1-48.
- Clarke, D. 1996. Zodiacal light – scattered Fraunhofer line profiles. In: *Physics, chemistry, and dynamics of interplanetary dust*, ed. B. A. S. Gustafson and M. S. Hanner, ASP Conference Series **104**, pp. 337-340.
- Clarke, D., Matthews, S. A., Mundell, C. G., and Weir, A. S. 1996. On the line profiles in the spectra of the zodiacal light. *Astron. Astrophys.* **308**, 273-278.
- Dermott, S. F., Grogan, K., Durda, D. D., Jayaraman, S., Kehoe, T. J. J., Kortenkamp, S. J., Wyatt, M. C. 2001. Orbital evolution of interplanetary dust. In: *Interplanetary dust*, ed. E. Grün, B. A. S. Gustafson, S. F. Dermott, and H. Fechtig. A&A library. Berlin: Springer-Verlag, 569-639.
- Dermott, S. F., Durda, D. D., Grogan, K., and Kehoe, T. J. J. 2002. Asteroidal dust. In: *Asteroids III*, ed. W. F. Bottke, Jr., A. Cellino, P. Paolicchi, and R. P. Binzel. Tucson: The University of Arizona Press, pp. 423-442.
- Dikarev, V., Rüdiger, J., and Grün, E. 2002. Towards a new model of the interplanetary meteoroid environment. *Adv. Space Res.* **29**, 1171-1175.
- East, I. R., and Reay, N. K. 1984. The motion of interplanetary dust particles. I - Radial velocity measurements on Fraunhofer line profiles in the Zodiacal Light spectrum. *Astron. Astrophys.*, **139**, 512-516.

- Fechtig, H., Leinert, C., and Berg, O. E. 2001. Historical perspectives. In: *Interplanetary dust*, ed. E. Grün, B. A. S. Gustafson, S. F. Dermott, and H. Fechtig. A&A library. Berlin: Springer-Verlag, pp. 1-55.
- Fernandez, Y. R., Jewitt, D. C., and Sheppard, S. S. 2005. Albedos of asteroids in comet-like orbits. *Astron. J.* **130**, 308-318.
- Fried, J. M. 1978. Doppler shifts in the zodiacal light spectrum. 1978. *Astron. Astrophys.* **68**, 259-264.
- Fixsen, D. and Dwek, E. 2002. The zodiacal emission spectrum as determined by COBE and its implications. *Astrophys. J.* **578**, 1009-1014.
- Giese, R. H. 1963. Light scattering by small particles and models of interplanetary matter derived from the zodiacal light. *Space Science Reviews* **1**, 589-611.
- Giese, R. H. and v. Dziembowski, C. 1969. Suggested zodiacal light measurement from space probes. *Planet. Space Sci.* **17**, 949-956.
- Gombosi, T. I., Cravens, T. E., and Nagy, A. F. 1985. Time-dependent dusty gasdynamical flow near cometary nuclei. *Astrophys. J.* **293**, 328-341.
- Gor’kavyi, N. N., Ozernoy, L. M., and Mather, J. C. 1997. A new approach to dynamical evolution of interplanetary dust. *Astrophys. J.* **474**, 496-502.
- Gor’kavyi, N., Ozernoy, L., Mather, J., and Taidakova, T. 1998. Structure of the zodiacal cloud: New analytical and numerical solutions. *Earth Planets Space* **50**, 539-544.
- Gorkavyi, N. N., Ozernoy, L. M., Taidakova, T., and Mather, J. C. 2000a. The NGST and the zodiacal light in the Solar system. *NGST Science and Technology Exposition*, ed. by E. P. Smith and K. S. Long, *ASP Series* **207**, 462-467. *astro-ph/9910551*.
- Gorkavyi, N. N., Ozernoy, L. M., Taidakova, T., and Mather, J. C. 2000b. Distribution of dust from Kuiper belt objects. *astro-ph/0006435*.
- Grogan, K., Dermott, S. F., and Durda, D. D. 2001. The size-frequency distribution of the zodiacal cloud: Evidence from the Solar System dust bands. *Icarus* **152**, 251-267.
- Grün, E. 1994. Dust measurements in the outer solar system. In: *Asteroids, Comets, Meteors 1993*, ed. by A. Milani, M. D. Martino, and A. Cellino. IAU N 160, Kluwer Academic Publ., Dordrecht, pp. 367-380.

- Grün, E., Fechtig, H., Kissel, J., and Gammel, P. 1977. Micrometeoroid data from the first two orbits of HELIOS 1. *J. Geophys.* **42**, 717-726.
- Grün, E., Zook, H. A., Fechtig, H., and Giese, R. H. 1985. Collisional balance of the meteoritic complex. *Icarus* **62**, 244-272.
- Grün, E., Kruger, H., and Landgraf, M. 2000. Dust Measurements in the Outer Solar System. In: *Minor bodies in the outer solar system*, ed. by A. Fitzsimmons, D. Jewitt, and R. M. West. Proc. of the ESO workshop held at Garching, Germany, 2-5 November 1998. Springer-Verlag, pp. 99-108.
- Grün, E., Baguhl, M., Svedhem, H., and Zook, H. A. 2001. In situ measurements of cosmic dust. In: *Interplanetary dust*, edited by E. Grün, B. A. S. Gustafson, S. Dermott, and H. Fechtig. A&A library, Springer-Verlag, Berlin, pp. 295-346.
- Grundy, W. M., Noll, K. S., and Stephens, D. C. 2005. Diverse albedos of small trans-Neptunian objects. *Icarus* **176**, 184-191.
- Hahn, J. M., Zook, H. A., Cooper, B., and Sunkara, B. 2002. Clementine observations of the zodiacal light and the dust content of the inner solar system. *Icarus* **158**, 360-378.
- Hanner, M. S., Sparrow, J. G., Weinberg, J. L., and Beeson, D. E. 1976. Pioneer 10 observations of zodiacal light brightness near the ecliptic: Changes with heliocentric distance. In: *Zodiacal light and interplanetary dust*, ed. H. Elsässer and H. Fechtig. Lecture Notes in Phys. **48**, Springer-Verlag, Heidelberg, pp. 29-35.
- Hicks, T. R., May, B. H., and Reay, N. K. 1974. An investigation of the motion of zodiacal dust particles - I. Radial velocity measurements on Fraunhofer line profiles. *Mon. Not. R. Astr. Soc.* **166**, 439-448.
- Hong, S. S., 1985. Henyey-Greenstein representation of the mean volume scattering phase function for zodiacal dust. *Astron. Astrophys.* **146**, 67-75.
- Humes, D. H. 1980. Results of Pioneer 10 and 11 meteoroid experiments: Interplanetary and near-Saturn. *J. Geophys. Res.* **85**, 5841-5852.
- Humes, D. H. 1993. Small craters on the meteoroid and space debris impact experiment. *NASA CP 3275*, Part 1, 287-322.
- Ipatov, S. I. and A'Hearn, M. F. 2006. Velocities of material ejected from Comet Tempel 1. *Lunar Planet. Sci.* **37**, #1462.

- Ipatov, S. I. and Mather, J. C. 2003. Migration of trans-Neptunian objects to the terrestrial planets. *Earth, Moon, and Planets* **92**, 89-98.
- Ipatov, S. I. and Mather, J. C. 2004a. Migration of Jupiter-family comets and resonant asteroids to near-Earth space. In: *Astrodynamics, Space Missions, and Chaos*, ed. by E. Belbruno, D. Folta, and P. Gurfil, New York: NYAS, *Annals of the New York Acad. of Sci.* **1017**, 46-65.
- Ipatov, S. I. and Mather, J. C. 2004b. Comet and asteroid hazard to the terrestrial planets. *Adv. Space Res.* **33**, 1524-1533.
- Ipatov, S. I. and Mather, J. C. 2006. Migration of small bodies and dust to near-Earth space. *Adv. Space Res.* **37**, 126-137.
- Ipatov, S. I. and Mather, J. C. 2007. Migration of dust particles to the terrestrial planets. In: *Dust in Planetary Systems*, ed. H. Kruger and A. Graps. ESA, SP 643, pp. 91-94.
- Ipatov, S. I., Mather, J. C., and Taylor, P. A. 2004. Migration of interplanetary dust. In: *Astrodynamics, Space Missions, and Chaos*, ed. by E. Belbruno, D. Folta, and P. Gurfil, New York: NYAS, *Annals of the New York Acad. of Sci.* **1017**, 66-80.
- Ipatov, S. I., Kutyrev, A. S., Madsen, G. J., Mather, J. C., Moseley, S. H., and Reynolds, R. J. 2005. Dynamical zodiacal cloud models constrained by high resolution spectroscopy of the zodiacal light. *Lunar Planet. Sci.* **36**, #1266.
- Ipatov, S. I., Kutyrev, A. S., Madsen, G. J., Mather, J. C., Moseley, S. H., and Reynolds, R. J. 2006. Dynamical zodiacal cloud models. *Lunar Planet. Sci.* **37**, #1471.
- James, J. F. 1969. Theoretical Fraunhofer line profiles in the spectrum of the zodiacal light. *Mon. Not. R. Astron. Soc.* **142**, 45-52.
- Jackson, A. A. and Zook, H. A. 1992. Orbital evolution of dust particles from comets and asteroids. *Icarus* **97**, 70-84.
- Jorda, L., Lamy, P., Faury, G., Keller, H. U., Hviid, S., Küppers, M., Koschny, D., Lecacheux, J., Gutierrez, P., and Lara, L. M. 2007. Properties of the dust cloud caused by the Deep Impact experiment. *Icarus* **187**, 208-219.
- Kehoe, T.J.J., Dermott, S.F., and Mahoney-Hopping, L.M. 2007. The effect of inter-particle collisions on the dynamical evolution of asteroidal dust and the structure of the zodiacal cloud. In: *Dust in Planetary Systems*, ed. H. Kruger and A. Graps. ESA, SP 643, pp. 81-85.

- Kelsall, T., Weiland, J. L., Franz, B. A., Reach, W. T., Arendt, R. G., Dwek, E., Freudenreich, H. T., Hauser, M. G., Moseley, S. H., Odegard, N. P., Silverberg, R. F., and Wright, E. L. 1998. The COBE diffuse infrared background experiment search for the cosmic infrared background. II. Model of the interplanetary dust cloud. *Astrophys. J.* **508**, 44-73.
- Kortenkamp, S. J. and Dermott, S. F. 1998. Accretion of interplanetary dust particles by the Earth. *Icarus* **135**, 469-495.
- Landgraf, M., Liou, J.-C., Zook, H. A., and Grün, E. 2002. Origins of solar system dust beyond Jupiter. *Astron. J.* **123**, 2857-2861.
- Lamy, P. L. and Perrin, J.-M. 1986. Volume scattering function and space distribution of the interplanetary dust cloud. *Astron. Astrophys.* **163**, 269-286.
- Leinert, C. 1975. Zodiacal light — a measure of interplanetary environment. *Space Sci. Rev.* **18**, 281-339.
- Leinert, C., Link, H., Pitz, E., and Giese, R. H. 1976. Interpretation of a rocket photometry of the inner zodiacal light, *Astron. Astrophys.* **47**, 221-230.
- Leinert, C., Richter, I., Pitz, E., and Plank, B. 1981. The zodiacal light from 1.0 to 0.3 A.U. as observed by the HELIOS space probes. *Astron. Astrophys.* **103**, 177-188.
- Levison, H. F. and Duncan, M. J. 1994. The long-term dynamical behavior of short-period comets. *Icarus* **108**, 18-36.
- Liou, J.-C. and Zook, H. A. 1999. Signatures of the giant planets imprinted on the Edgeworth-Kuiper belt dust disk. *Astron. J.* **118**, 580-590.
- Liou, J.-C., Dermott, S. F., and Xu, Y. L. 1995. The contribution of cometary dust to the zodiacal cloud. *Planet. Space Sci.* **43**, 717-722.
- Liou, J.-C., Zook, H. A., and Dermott, S. F. 1996. Kuiper belt dust grains as a source of interplanetary dust particles. *Icarus* **124**, 429-440.
- Liou, J.-C., Zook, H. A., and Jackson, A. A. 1999. Orbital evolution of retrograde interplanetary dust particles and their distribution in the Solar system. *Icarus* **141**, 13-28.
- Lisse, C. M., Fernandez, Y. R., A'Hearn, M. F., Grün, E., Käufel, H. U., Osip, D. J., Lien, D. J., Kostiuk, T., Peschke, S. B., Walker, R. G. 2004. A tale of two very different comets: ISO and MSX measurements of dust emission from 126P/IRAS (1996) and 2P/Encke (1997). *Icarus* **171**, 444-462.



- Love, S. G. and Brownlee, D. E. 1993. A Direct measurement of the terrestrial mass accretion rate of cosmic dust. *Science* **262**, 550-553.
- Madsen, G. J., Reynolds, R. J., Ipatov, S. I., Kutyrev, A. S., Mather, J. C., and Moseley, S. H. 2007. New observations and models of the kinematics of the zodiacal dust cloud. In: *Dust in Planetary Systems*, ed. H. Kruger and A. Graps. ESA, SP 643, pp. 61-64.
- Moro-Martin, A. and Malhotra, R. 2002. A study of the dynamics of dust from the Kuiper belt: Spatial distribution and spectral energy distribution. *Astron. J.* **124**, 2305-2321.
- Moro-Martin, A. and Malhotra, R. 2003. Dynamical models of Kuiper belt dust in the inner and outer solar system. *Astron. J.* **125**, 2255-2265.
- Nagel, K. and Fechtig, H. 1980. Diameter to depth dependence of impact craters. *Planet. Space Sci.* **28**, 567-569.
- Nesvorný, D., Vokrouhlický, D., Bottke, W.F., and Sykes, M. 2006. Physical properties of asteroid dust bands and their sources. *Icarus* **181**, 107-144.
- Ozernoy, L. M. 2001. Physical modeling of the zodiacal dust cloud. In: *The extragalactic infrared background and its cosmological implications*, ed. M. Harwit and M. G. Hauser. IAU Symp. No. 204, ASP Conference Series, pp. 17-34. *astro-ph/0012033*.
- Reach, W. T. 1991. Zodiacal emission. II. Dust near ecliptic. *Astrophys. J.* **369**, 529-543.
- Reach, W. T. 1992. Zodiacal emission. III. Dust near the asteroid belt. *Astrophys. J.* **392**, 289-299.
- Reach, W. T., Franz, B. A., and Weiland, J. L. 1997. The three-dimensional structure of the zodiacal dust bands. *Icarus* **127**, 461-484.
- Reynolds, R. J., Madsen, G. J., and Moseley, S. H. 2004. New measurements of the motion of the zodiacal dust. *Astrophys. J.* **612**, 1206-1213.
- Schuerman, D. W. 1979. Inverting the zodiacal light brightness integral. *Planet. Space Sci.* **27**, 551-556.
- Sekanina, Z. 1987. Dust environment of Comet P/Halley — A review. *Astron. Astrophys.* **187**, 789-795.
- Southworth, R. B. 1964. In: *Cosmic Dust*, ed. H. E. Whipple, New York: NYAS, *Annals of the New York Acad. of Sci.* **119**, 54-67.

- Sykes, M. V., Grün, E., Reach, W. T., and Jenniskens, P. 2004. The interplanetary dust complex and comets. In: *Comets II*, ed. M. Festou, H. U. Keller, and H. A. Weaver, University of Arizona Press, pp. 677-693.
- Vedder, J. F. and Mandeville, J.-C. 1974. Microcraters formed in glass by projectiles of various densities. *J. Geophys. Res.* **79**, 3247-3256.
- Weiss-Wrana, K. 1983. Optical properties of interplanetary dust — Comparison with light scattering by larger meteoritic and terrestrial grains. *Astron. Astrophys.* **126**, 240-250.
- Wyatt, M. C. 2005. The origin and evolution of dust belts. In: *Dynamics of populations of planetary systems*, ed. by Z. Knezevic and A. Milani, IAU Colloq. N 197 (Belgrade, Serbia and Montenegro, 31 Aug. - 4 Sept., 2004), Cambridge University Press, pp. 383-392.
- Zook, H. A. 2001. Spacecraft measurements of the cosmic dust flux. In: *Accretion of extraterrestrial matter throughout Earth's history*, ed. by B. Peucker-Ehrenbrink and B. Schmitz, Kluwer, New York, pp. 75-92.

Table 1: Fractions of asteroidal, cometary, and trans-Neptunian particles among zodiacal dust, constrained by different observations (see details in Introduction)

References	Observations used	Fraction of asteroidal dust	Fraction of cometary dust	Fraction of trans-Neptunian dust
Zook 2001	Cratering rates from Earth- and Lunar-orbiting satellites		0.75	
Liou et al. 1995	IRAS observations of the shape of zodiacal cloud		0.67-0.75	
Gorkavyi et al. 2000; Ozerney 2001	COBE/DIRBE observations of brightness vs. latitude	0.30	0.36	0.34
Grogan et al. 2001; Dermott et al. 2001; Wyatt 2005	dust bands	>0.3		
Dermott et al. 2002	dust bands	most		
Brownlee et al. 1973; Vedder and Mandeville 1974; Fechtig et al. 2001	shape of microcraters	>0.7		
Nesvorný et al. 2006	IRAS observations of dust bands	0.05-0.09 for Karin/Veritas particles	dominated by high-speed cometary particles	
Present paper	WHAM observations and observations of number density	0.3-0.5	0.4-0.7	$\leq 0.1$

Table 2: Characteristic velocity amplitude  $v_a$  of ‘velocity-elongation’ curves at  $90^\circ < \epsilon < 270^\circ$ , minimum ( $v_{\min}$ ) and maximum ( $v_{\max}$ ) velocities at the above interval, mean eccentricities ( $e_z$ ) and mean inclinations ( $i_z$ ) at distance from the Sun  $1 \leq R \leq 3$  AU for particles from different sources at intervals of  $\beta$

Source of particles	$\beta$	$e_z$	$i_z$ (deg.)	$v_a$ (km s <sup>-1</sup> )	$v_{\min}$ (km s <sup>-1</sup> )	$v_{\max}$ (km s <sup>-1</sup> )
asteroids	0.0004-0.1	<0.3	8-13	9	(-13)-(-11)	5-7
asteroids	0.0001	0.2-0.3	7-14	13	-15	11
10P	0.0001-0.2	0.2-0.6	7-13	8	(-11)-(-9)	3-9
39P	0.01-0.2	0.2-0.4	10-14	8-9	(-13)-(-9)	4-8
39P	0.0001-0.004	0.3-0.8	15-24	11-17	(-20)-(-10)	8-16
2P	0.01-0.1	0.5-0.8	7-23	13	(-12)-(-7)	12-22
2P	0.0001-0.004	0.7-0.9	8-15	14	(-16)-(-12)	15-20
2P 0.25t	0.002-0.2	0.6-0.85	4-11	16	(-14)-4	12-40
2P 0.5t	0.002-0.4	0.5-0.85	4-11	14	(-22)-(-2)	2-29
tn	0.05-0.4	0.1-0.4	11-23	16	(-20)-(-14)	12-18
tn	0.002-0.01	0.4-0.8	9-33	12	-16	8
lp, $q=0.9$ AU	0.002	0.2-0.9	55-155	41	-44	38
lp, $q=0.9$ AU	0.0001-0.001	0.8-1.	80-115	33	(-38)-(-32)	28-34
lp, $q=0.1$ AU	0.0004	0.95-1.	95-105	34	-34	34
ht, $q=0.5$ AU	0.001-0.012	0.45-1.	95-135	37	-35	40

FIGURE CAPTIONS:

Fig. 1. Dependence of the intensity of light vs. its wavelength  $\lambda$  (in Angstrom) at  $\beta=0.2$ ,  $\epsilon=180^\circ$ , in the ecliptic plane (a) and at  $\beta=0.05$  (exclusive for  $lp$  particles considered at  $\beta=0.002$ ) toward the North Ecliptic Pole (b). Zero of  $\Delta\lambda=\lambda-\lambda_o$  corresponds to  $\lambda=\lambda_o=5183.62$  Angstrom. The plots for dust particles produced by asteroids, trans-Neptunian objects, Comet 2P at perihelion, Comets 10P and 39P are denoted by ‘ast’, ‘tn’, ‘2P’, ‘10P’, and ‘39P’, respectively. Data for particles originating from long-period comets at  $e_o=0.995$ ,  $q_o=0.9$  AU, and  $i_o$  distributed between 0 and  $180^\circ$ , are marked as ‘lp’. Marks in Fig. (a) are for average intensity for observations at  $174^\circ \leq \epsilon \leq 188^\circ$ , and marks in Fig. (b) are for average observations toward the North Ecliptic Pole. Coordinates of marks for ‘observ/sol spectr’ were obtained from observational data by making it have the same minimum value as the solar spectrum. The minima of plots obtained in all calculations were made the same as that for the solar spectrum.

Fig. 2. Velocities of Mg I line (at zero inclination) versus elongation  $\epsilon$  (measured eastward from the Sun) at  $\beta=0.05$  for dust particles produced by asteroids (a), Comet 2P/Encke at perihelion (b). Letter ‘c’ denotes the model for which the shift of the curve of  $I$  versus  $\epsilon$  is calculated as a shift of centroid, and letter ‘m’ denotes the model for which the shift of the curve is calculated as a shift of the minimum of the curve. The number after ‘m’ or ‘c’ characterizes the number of a scattering function used.

Fig. 3. Velocities of Mg I line (at zero inclination) versus elongation  $\epsilon$  (measured eastward from the Sun) at several values of  $\beta$  (see the last number in the legend) for particles produced by asteroids (a-b) and Comet 10P/Tempel 2 (c-d). The line corresponds to the observations made by Reynolds et al. (2004).

Fig. 4. Velocities of Mg I line (at zero inclination) versus elongation  $\epsilon$  (measured eastward from the Sun) at several values of  $\beta$  for particles produced by Comet 2P/Encke at perihelion (a-b), for particles launched from Comet 39P/Oterma (c-d), for particles originating from trans-Neptunian objects (e), test long-period comets (‘lp’) at  $e_o=0.995$ ,  $q_o=0.9$  AU, and  $i_o$  distributed between 0 and  $180^\circ$ , test long-period comets (‘lpc’) at  $e_o=0.999$ ,  $q_o=0.1$  AU, and  $i_o$  distributed between 0 and  $180^\circ$ , and test Halley-type comets (‘ht’) at  $e_o=0.975$ ,  $q_o=0.5$  AU, and  $i_o$  distributed between 0 and  $180^\circ$  (f). The line corresponds to the observations made by Reynolds et al. (2004).

Fig. 5. Mean value of the width of Mg I line (in the ecliptic plane) for elongation  $\epsilon$  between  $30^\circ$  and  $330^\circ$  at several values of  $\beta$  for particles originating from asteroids (ast), from Comet 2P/Encke at perihelion (2P), at the middle of the orbit (2P 0.25t), and at aphelion (2P 0.5t), from Comets 10P/Tempel 2 and 39P/Oterma (10P and 39P), from test

long-period comets (lp) at  $e_o=0.995$ ,  $q_o=0.9$  AU, and  $i_o$  distributed between 0 and  $180^\circ$ , and from test Halley-type comets (ht) at  $e_o=0.975$ ,  $q_o=0.5$  AU, and  $i_o$  distributed between 0 and  $180^\circ$ . Solid line corresponds to the observational value.

Fig. 6. Mean eccentricity of particles at different distances from the Sun at several values of  $\beta$  (see the last number in the legend) for particles originating from asteroids (ast), from Comet 2P/Encke at perihelion (2P), from Comets 10P/Tempel 2 and 39P/Oterma (10P and 39P), from trans-Neptunian objects (tn), from test long-period comets (lp) at  $e_o=0.995$ ,  $q_o=0.9$  AU, and  $i_o$  distributed between 0 and  $180^\circ$ , from test long-period comets (lpc) at  $e_o=0.999$ ,  $q_o=0.1$  AU, and  $i_o$  distributed between 0 and  $180^\circ$ , and from test Halley-type comets (ht) at  $e_o=0.975$ ,  $q_o=0.5$  AU, and  $i_o$  distributed between 0 and  $180^\circ$ .

Fig. 7. Mean orbital inclination (in degrees) of particles at different distances from the Sun at several values of  $\beta$  (see the last number in the legend) for particles originating from asteroids (ast), from Comet 2P/Encke at perihelion (2P), from Comets 10P/Tempel 2 and 39P/Oterma (10P and 39P), from trans-Neptunian objects (tn), from test long-period comets (lp) at  $e_o=0.995$ ,  $q_o=0.9$  AU, and  $i_o$  distributed between 0 and  $180^\circ$ , from test long-period comets (lpc) at  $e_o=0.999$ ,  $q_o=0.1$  AU, and  $i_o$  distributed between 0 and  $180^\circ$ , and from test Halley-type comets (ht) at  $e_o=0.975$ ,  $q_o=0.5$  AU, and  $i_o$  distributed between 0 and  $180^\circ$ .

Fig. 8. Values of  $\alpha$  in  $n(R)\propto R^{-\alpha}$  obtained by comparison of the values of the number density  $n(R)$  at distance  $R$  from the Sun equal to 0.3 and 1 AU (a), at  $R=0.8$  and  $R=1.2$  AU (b), and at  $R$  equal to 1 and 3 AU (c). The values are presented at several values of  $\beta$  for particles originating from Comets 10P/Tempel 2 and 39P/Oterma (10P and 39P), from trans-Neptunian objects (tn), from test long-period comets (lp) at  $e_o=0.995$ ,  $q_o=0.9$  AU, and  $i_o$  distributed between 0 and  $180^\circ$ , and from test Halley-type comets (ht) at  $e_o=0.975$ ,  $q_o=0.5$  AU, and  $i_o$  distributed between 0 and  $180^\circ$ . Horizontal bars correspond to observations.

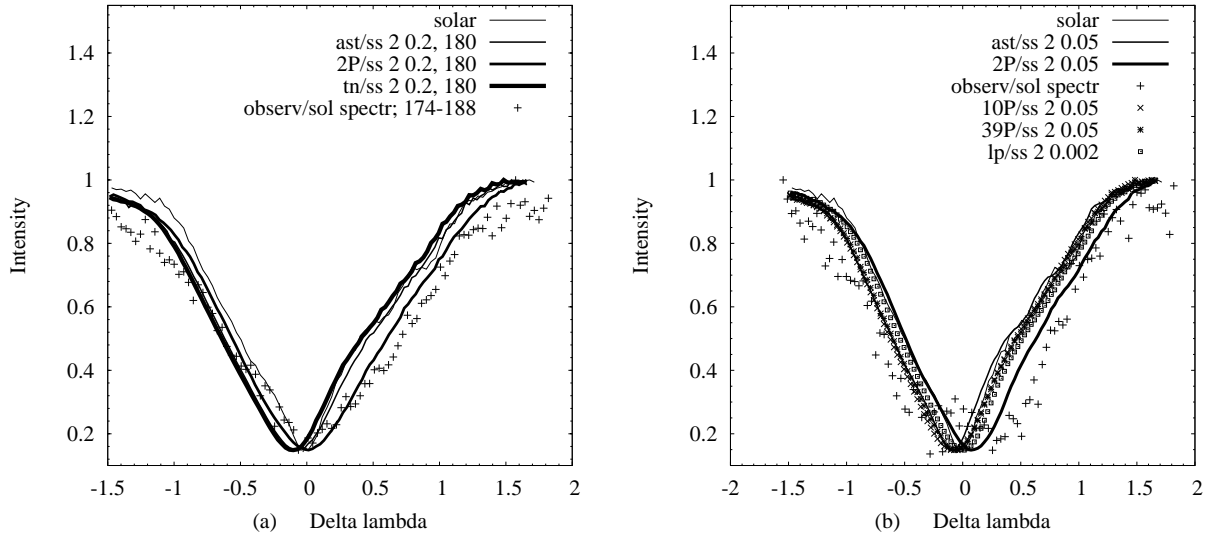


Fig. 1.— Ipatov et al., Zodiacal cloud...

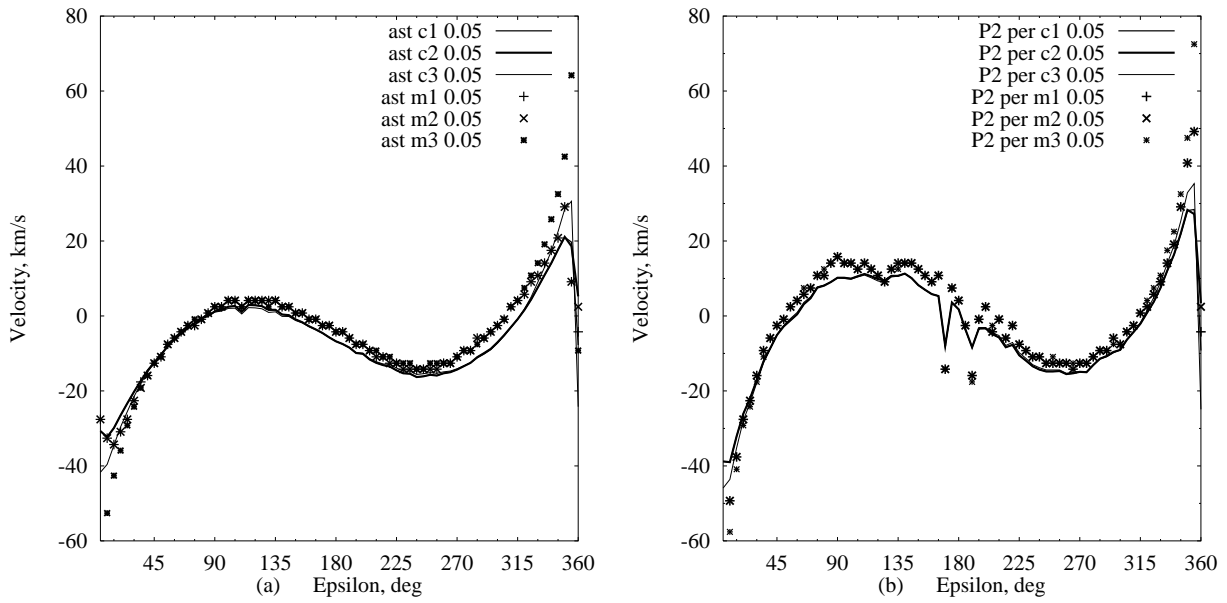


Fig. 2.— Ipatov et al., Zodiacal cloud...

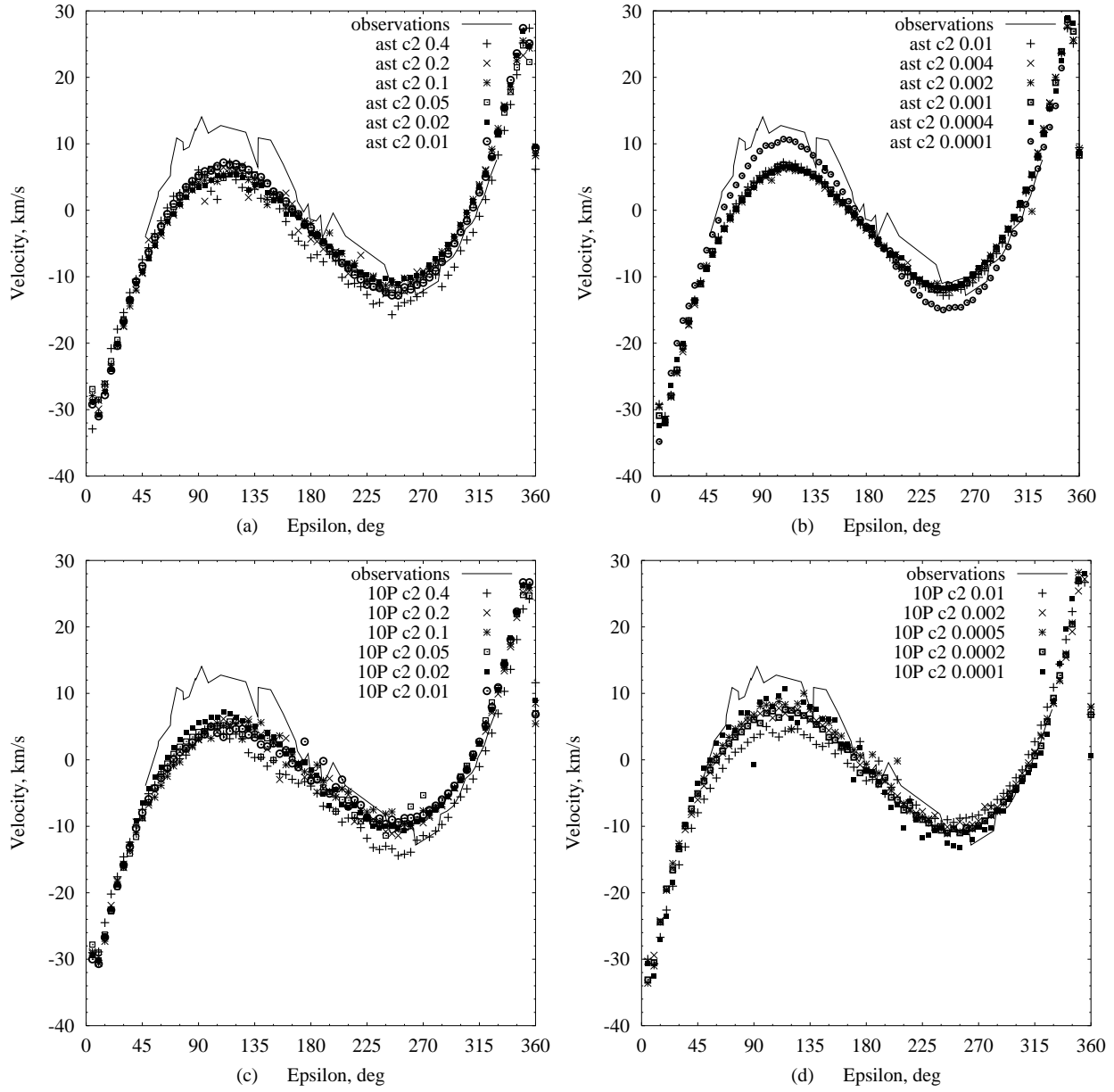
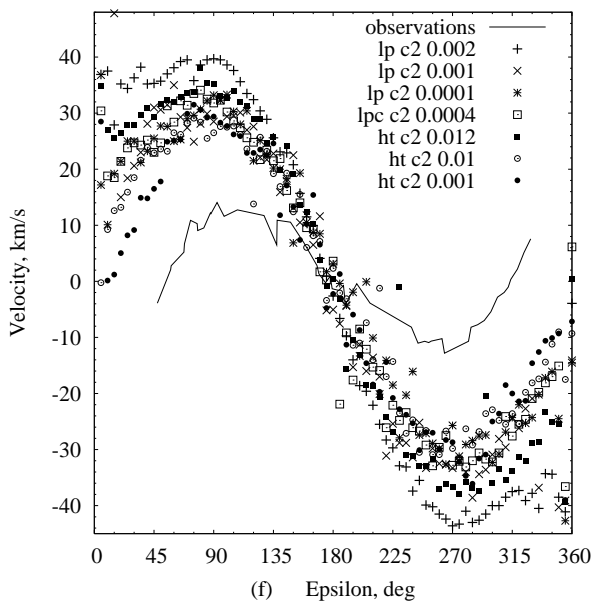
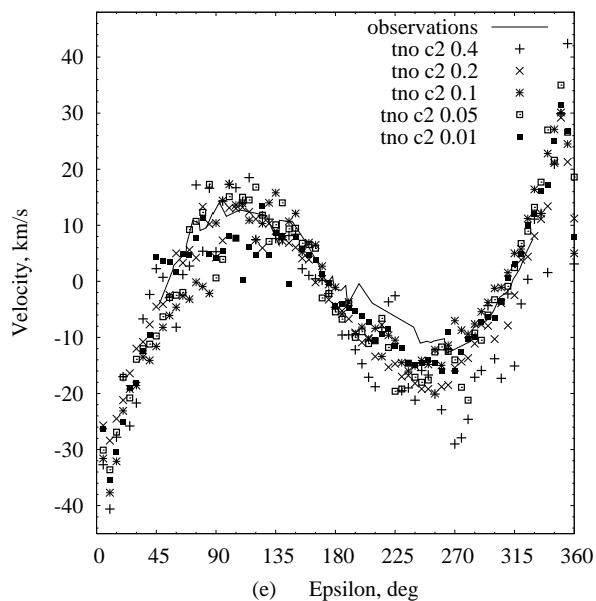
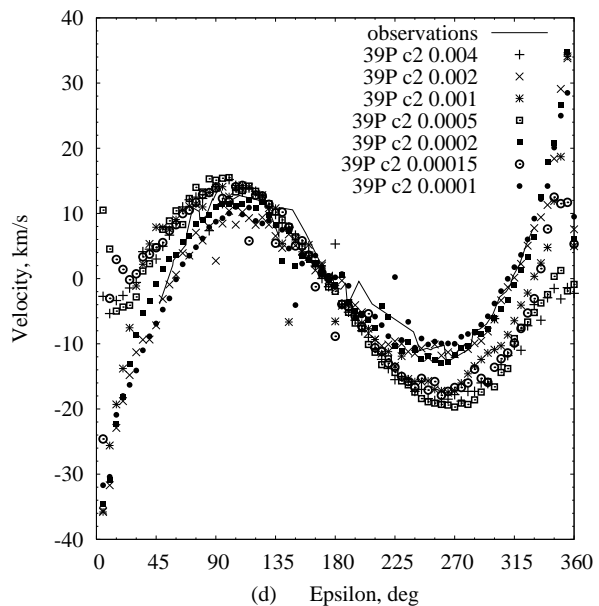
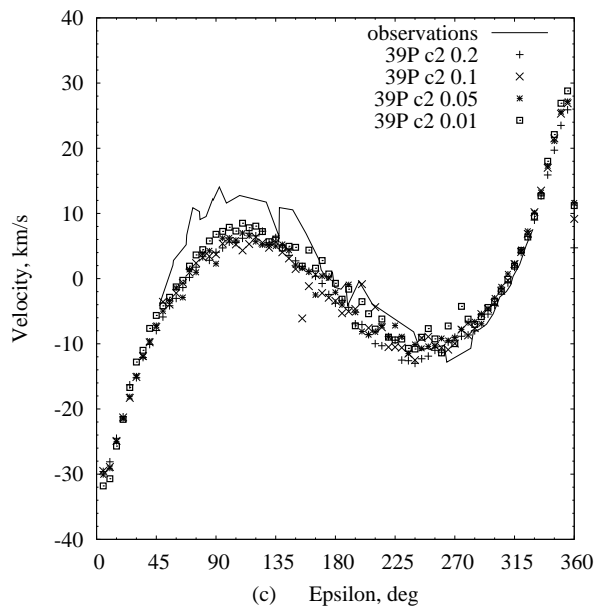
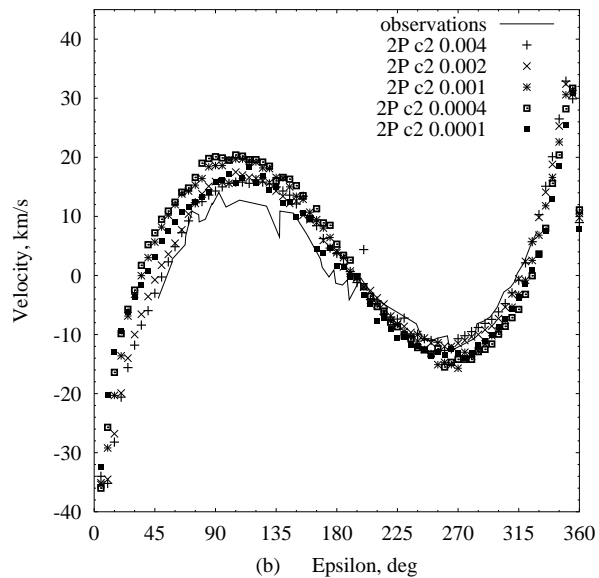
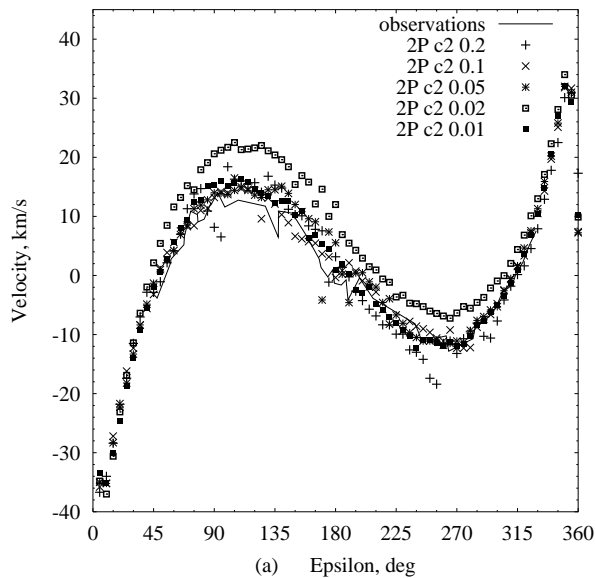


Fig. 3.— Ipatov et al., Zodiacal cloud...





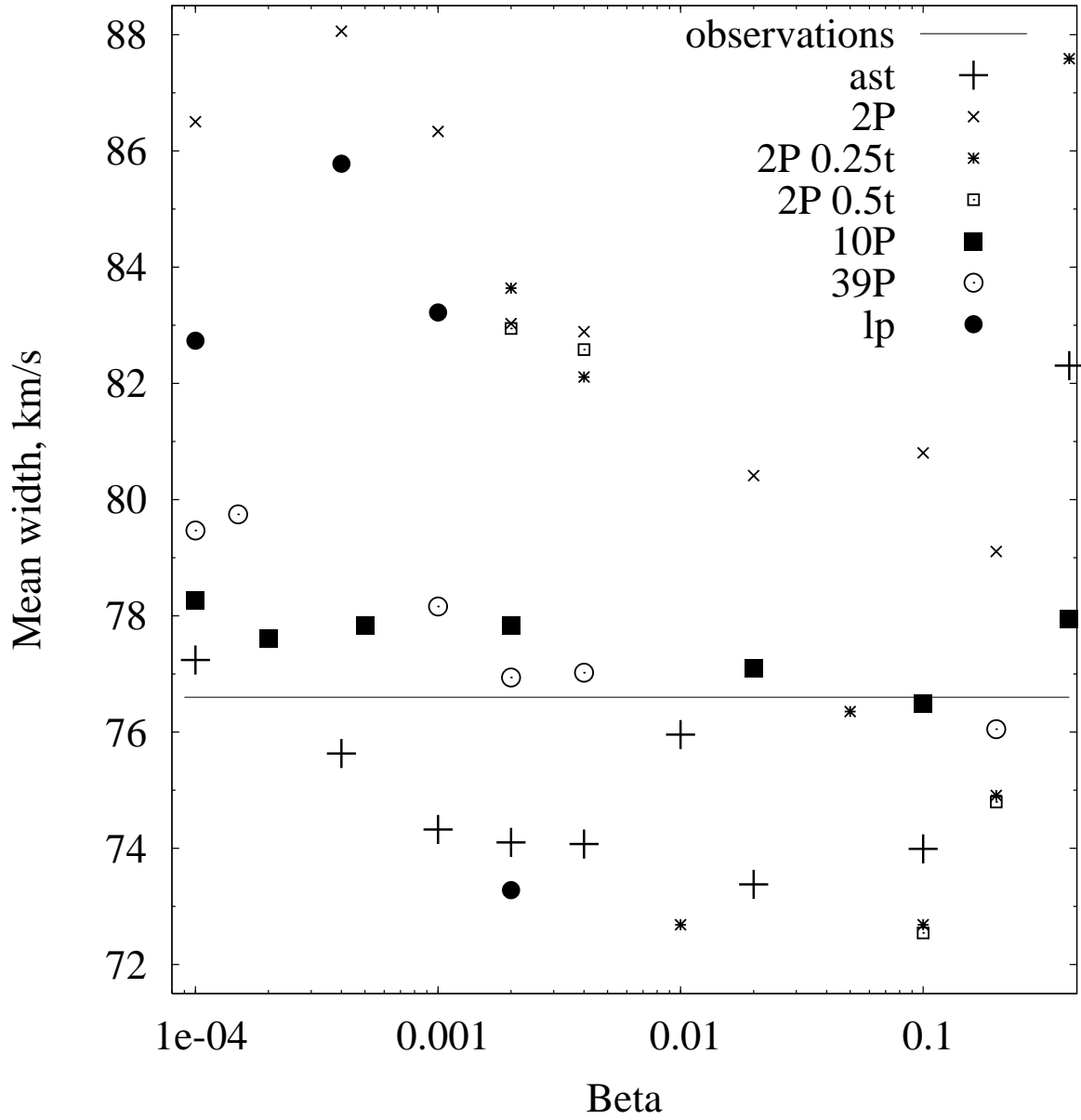
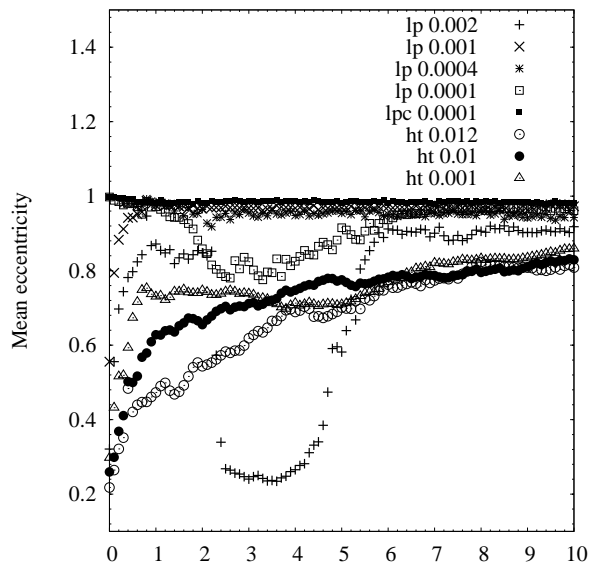
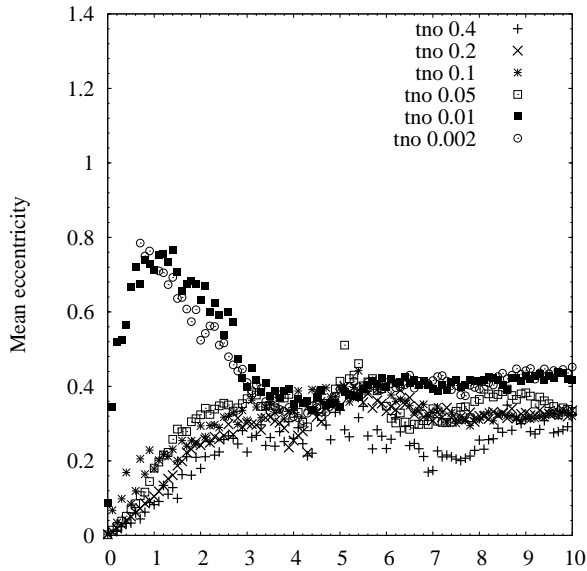
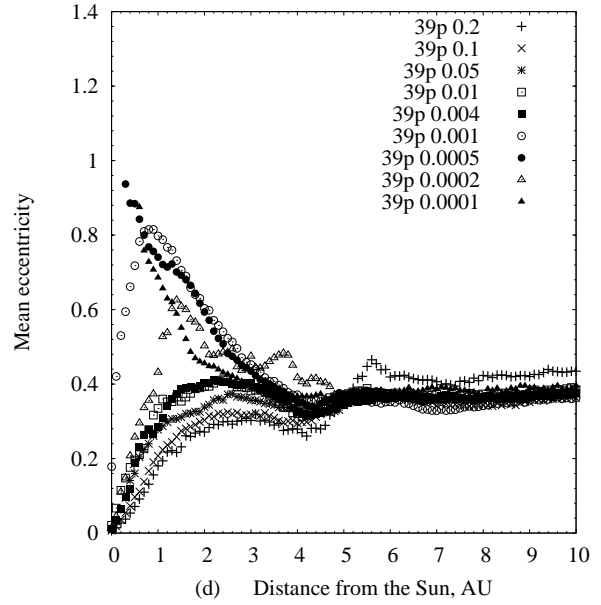
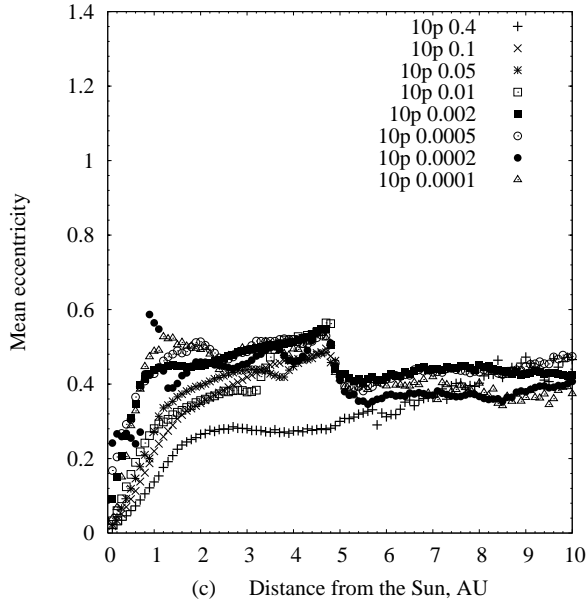
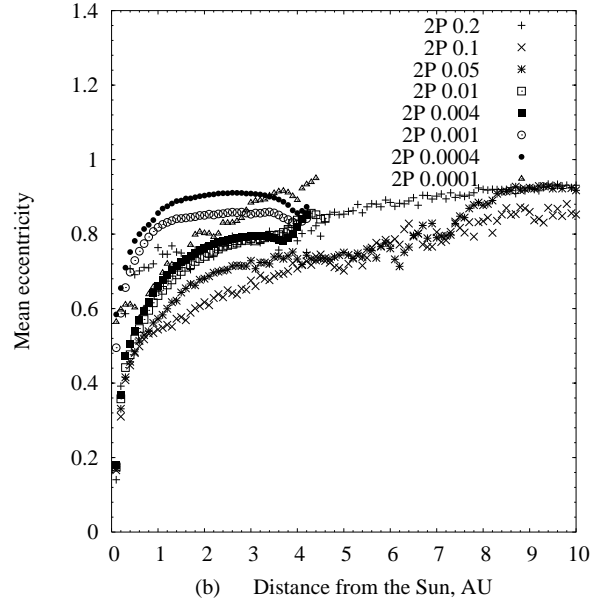
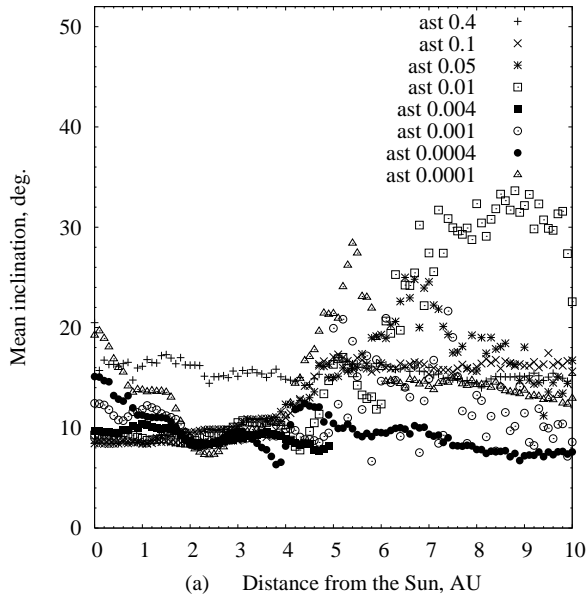
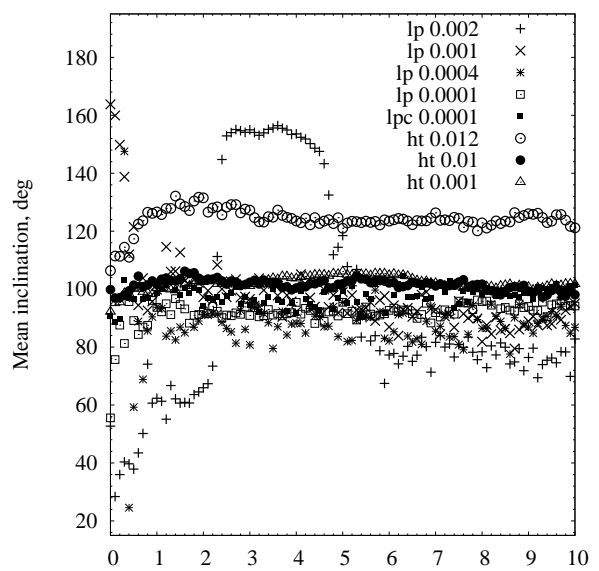
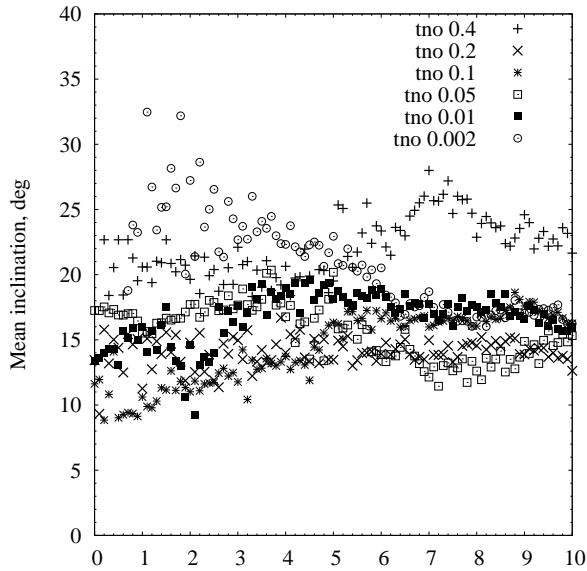
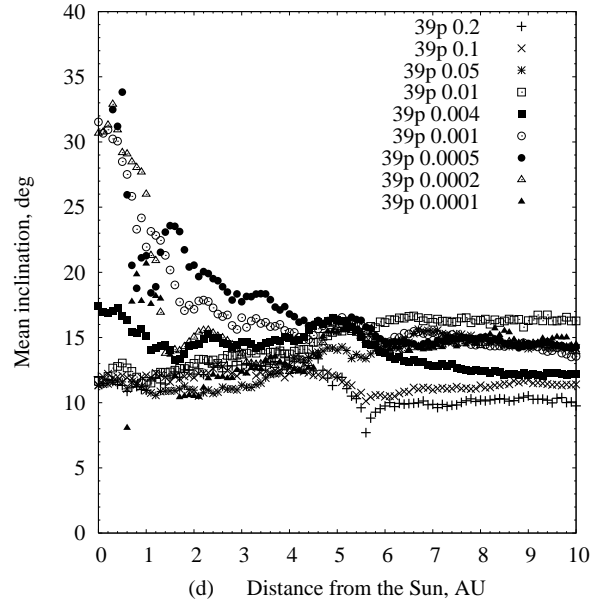
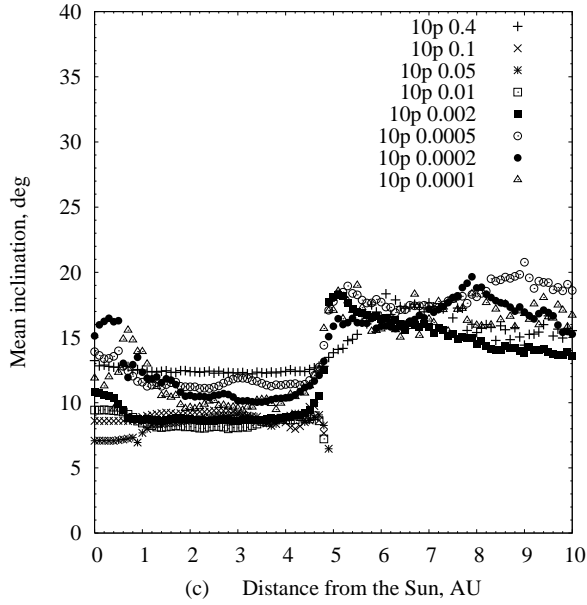
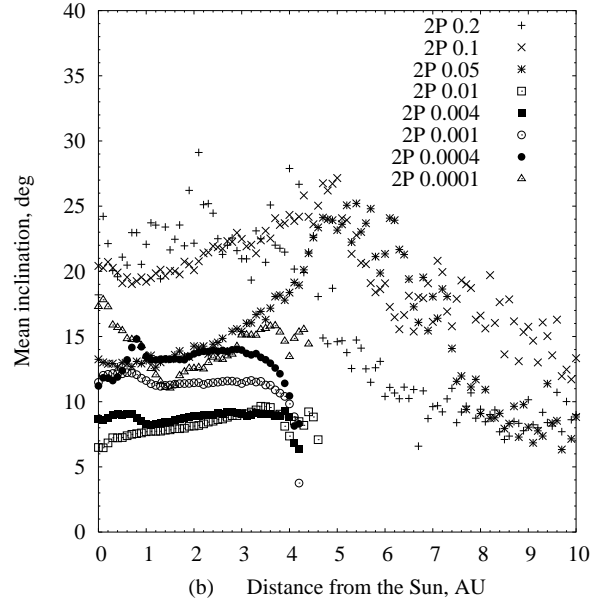
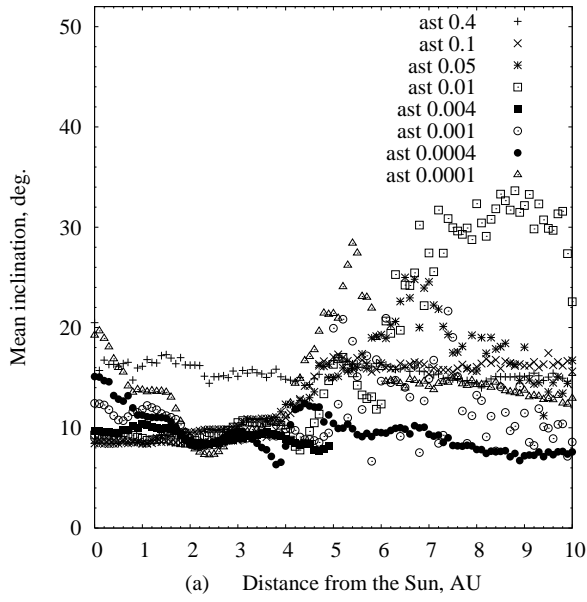


Fig. 5.— Ipatov et al., Zodiacal cloud...





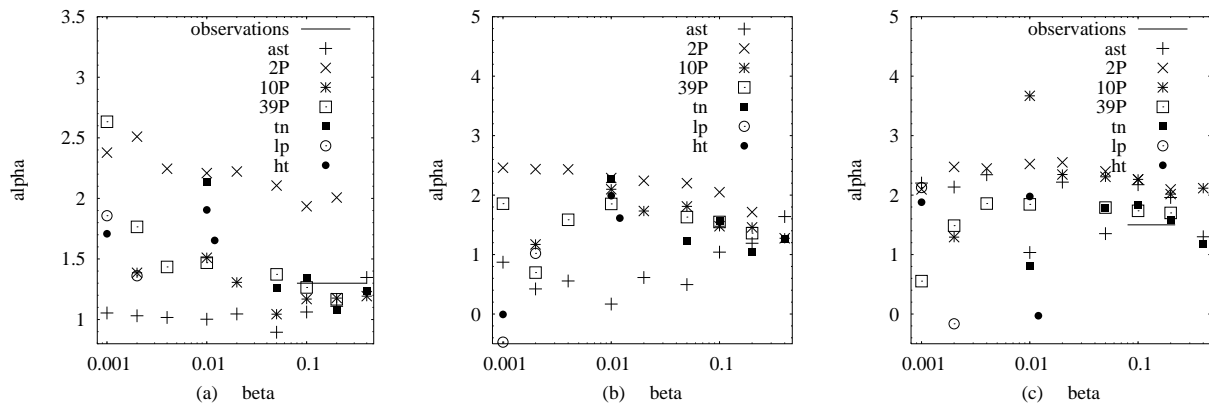


Fig. 8.— Ipatov et al., Zodiacal cloud...